Roles of Drop Size Distribution and Turbulence in Autoconversion Based on Lagrangian Cloud Model Simulations

Donggun Oh[1] and Yign Noh[2]

[1]Unknown
[2]Yonsei University

November 26, 2022

Abstract

The roles of the drop size distribution (DSD) and turbulence in the autoconversion rate A are investigated by analyzing Lagrangian cloud model (LCM) data for shallow cumulus clouds. The correlations of DSD and turbulence with other cloud parameters are estimated, and they are applied to parameterize their effects on A. A new parameterization of A is proposed based on it, as A = αqc7/3Nc-1/3H(Rc-Rc0) with α = aNc-X(Rc-Rc0)(1+bε), where qc, Nc, and Rc are the mixing ratio, the number concentration, and the volume mean radius of cloud droplets, respectively. ε is the dissipation rate, Rc0 is the threshold value of Rc, H is the Heaviside step function, and X, a, and b are constants. Here, Nc-X(Rc-Rc0) represents the effect of DSD, via its correlation with Nc and qc, while A [?] qc7/3Nc-1/3 represents the effect of the gravitational collisional growth for given DSD and turbulence. The correlation between turbulence and DSD makes b larger than expected based on turbulence-induced collision enhancement. The effects of DSD and turbulence and their correlations with qc and Nc explain a wide range of exponent values of qc and Nc in many existing parameterizations of A. The new parameterization is compared with the LCM data and applied to a bulk cloud model (BCM) while clarifying the difference between the cloud droplet mixing processes of the LCM and BCM. The importance of DSD and turbulence in the raindrop formation in shallow cumulus clouds are shown by comparing the results from A with and without these effects.

Roles of Drop Size Distribution and Turbulence in Autoconversion Based on Lagrangian Cloud Model Simulations

Enter authors here: D. Oh[1], Y. Noh[1]

[1]Department of Atmospheric Sciences, Yonsei University, Seoul, S. Korea.

Corresponding author: Yign Noh (noh@yonsei.ac.kr)

Key Points:

- Identification of the role of the drop size distribution and turbulence in autoconversion by analyzing Lagrangian cloud model data
- Correlations of the drop size distribution and turbulence with other cloud parameters and its application to the parameterization
- Development of a new parameterization of autoconversion and its application to a bulk cloud model

Abstract

The roles of the drop size distribution (DSD) and turbulence in the autoconversion rate *A* are investigated by analyzing Lagrangian cloud model (LCM) data for shallow cumulus clouds. The correlations of DSD and turbulence with other cloud parameters are estimated, and they are applied to parameterize their effects on *A*. A new parameterization of *A* is proposed based on it, as $A = \alpha q_c^{7/3} N_c^{-1/3} H(R_c - R_{c0})$ with $\alpha = a N_c^{-X}(R_c - R_{c0})(1 + b\varepsilon)$, where q_c, N_c, and R_c are the mixing ratio, the number concentration, and the volume mean radius of cloud droplets, respectively. ε is the dissipation rate, R_{c0} is the threshold value of R_c, *H* is the Heaviside step function, and *X*, a, and b are constants. Here, $N_c^{-X}(R_c - R_{c0})$ represents the effect of DSD, via its correlation with N_c and R_c, while $A \propto q_c^{7/3} N_c^{-1/3}$ represents the effect of the gravitational collisional growth for given DSD and turbulence. The correlation between turbulence and DSD makes *b* larger than expected based on turbulence-induced collision enhancement. The effects of DSD and turbulence and their correlations with q_c and N_c explain a wide range of exponent values of q_c and N_c in many existing parameterizations of *A*. The new parameterization is compared with the LCM data and applied to a bulk cloud model (BCM) while clarifying the difference between the cloud droplet mixing processes of the LCM and BCM. The importance of DSD and turbulence in the raindrop formation in shallow cumulus clouds are shown by comparing the results from *A* with and without these effects.

Plain Language Summary

One of the most important aspects of numerical weather prediction is to predict how much precipitation is generated from cloud droplets within a cloud; this process is referred to as autoconversion. Although autoconversion is known to be determined by the mass and number concentration of cloud droplets, it can also be affected by other factors, such as the drop size distribution (DSD) and turbulence. We clarify the effects of DSD and turbulence on autoconversion by analyzing the results of a realistic cloud field simulated by a new type of cloud model, in which cloud droplets are simulated as Lagrangian particles, and propose a parameterization to predict the autoconversion rate. It is found that the correlations of DSD and turbulence with other cloud parameters must be considered for the parameterization of their effects in autoconversion. We also apply the new parameterization to numerical weather prediction, and show that the DSD and turbulence play an important role in raindrop formation in shallow cumulus clouds.

1 Introduction

The parameterization of autoconversion, which calculates the rate of raindrop formation by the coalescence of two cloud droplets, plays a critical role in cloud microphysics parameterization, as it triggers precipitation. Nonetheless, it still remains one of the most uncertain parts of cloud microphysics parameterization. In most parameterizations, the rate of autoconversion *A* is expressed in terms of the mixing ratio and the number concentration of cloud droplets, q_c and N_c, respectively, as

$$A = \alpha q_c^m N_c^{-n} \Phi . \tag{1}$$

Here, α is a proportional constant and Φ is an additional multiplicative function (Table 1). In many parameterizations, $\Phi = 1$ (Beheng, 1994; Khairoutdinov & Kogan, 2000; Kogan, 2013), but in some parameterizations, Φ represents a threshold function such as $H(R_c - R_{c0})$ (Liu & Daum, 2004; Tripoli & Cotton, 1980), the influence of the drop size distribution (DSD) (Berry & Reinhardt, 1974; Liu & Daum, 2004; Liu et al., 2007; Seifert & Beheng, 2001), or the influence of turbulence (Seifert et al., 2010). Here, R_c is the volume mean radius of cloud droplets, which is defined as $q_c = (4\pi\rho_w / 3\rho_a) R_c^3 N_c$, R_{c0} is its threshold value, ρ_w and ρ_a are the density of water and air, respectively, and *H* is the Heaviside step function. Wide value ranges are suggested for *m* and *n*, i.e., *m* = 2.33-4.7 and *n* = 0.33-3.3. Accordingly, *A* varies greatly across different schemes, and this often causes discrepancies of several orders of magnitude (Menon et al., 2003; Wood, 2005; Hsieh et al., 2009).

A large number of previous works have attempted to clarify the roles of various processes in autoconversion, such as broadening of DSD (Baker et al., 1980; Blyth, 1993; Cooper, 1989; Lasher-Trapp et al., 2005) and turbulence-induced collision enhancement (TICE) (Franklin, 2008; Pinsky & Khain, 2002; Wang & Grabowski, 2009). Attempts have been made to incorporate the effects of these processes into the parameterization of autoconversion; for example, Seifert et al. (2010), Franklin (2008), and Seifert and Onishi (2016) studied TICE, and Berry and Reinhardt (1974), Liu and Daum (2004), and Milbrandt and Yau (2005a, b) examined the DSD. Wang and Grabowski (2009) showed that TICE could help overcome the delayed initiation of precipitation. Noh et al. (2018) showed that the effect of DSD could explain the so-called aging period problem associated with rainwater production that occurs too early and too low in a cloud (Shipway & Hill, 2012; Straka & Rasmussen, 1997).

	$A = \alpha q_c^m N_c^{-n} \Phi$		
	m	n	Φ
Kessler (1969)	1	0	$H(q_c - q_{c0})$
Tripoli and Cotton (1980)	7/3	1/3	$H(R_c - R_{c0})$
Beheng (1994)	4.7	3.3	1
Khairoutdinov and Kogan (2000)	2.47	1.79	1
Kogan (2013)	4.22	3.01	1
Liu and Daum (2004)	3	1	$f(\sigma_c / R_c) H(R_6 - R_{60})$
Liu et al. (2007)	3	1	$f(\sigma_c / R_c, q_c^{-2} N_c^{3/2})$
Berry and Reinhardt (1974)	2	0	$(R_c^4 - c_1)(R_c - c_2)$
Seifert and Beheng (2001)	4	2	$\tau^{0.68}(1-\tau^{0.68})^3$
Seifert et al. (2010)	4	2	$\tau^{0.68}(1-\tau^{0.68})^3(1+b\varepsilon)$
			$b = \mathrm{Re}_\lambda^{1/4} f(\overline{r}_c)$

Table 1 List of the parameterizations of A (R_6 = the mean radius of the sixth moment of the droplets, τ = internal time scale (q_r / q_l), Re_λ = Taylor microscale Reynolds number, $\overline{r}_c$ = mean radius of the cloud droplets, and c_1, c_2 = constants).

Considering the difficulty of obtaining reliable observation data, a widely used approach for evaluating cloud microphysics parameterizations is to analyze the results obtained from a box collision model, which calculates the evolution of the droplet spectrum induced by collision by solving the stochastic collection equation (SCE), used for a spectral bin model (SBM), based on a given initial DSD. For the initial DSD, observed DSD data (Hsieh et al., 2009; Wood, 2005) or an idealized DSD, such as a gamma or lognormal distribution (Berry & Rheinhardt, 1974; Franklin, 2008; Lee & Baik, 2017; Noh et al., 2018; Seifert & Beheng, 2001; Seifert et al., 2010) are used.

Many parameters used in cloud microphysics parameterizations, such as DSD and turbulence, are correlated with each other in real clouds. In a box collision model, however, it is difficult to consider these correlations, and thus these parameters are often regarded as independent. One way to cope with this problem is to use large eddy simulation (LES), in which the evolution of the DSD and the correlations between parameters are naturally reproduced during the evolution of clouds. Khairoutdinov and Kogan (2000) and Kogan (2013) analyzed data obtained from warm cloud fields simulated by LES coupled with an SBM for the parameterization of autoconversion, but they did not consider the effects of DSD, turbulence, and correlations of parameters.

Lagrangian cloud models (LCMs) have recently received much attention as a new type of cloud model (e.g., Andrejczuk et al., 2008, 2010; Arabas et al., 2015; Dziekan et al., 2019; Hoffmann et al., 2017; Riechelmann et al., 2012; Shima et al., 2009; Sölch & Kärcher, 2010). In such a model, the flow field is simulated by LES, and droplets are treated as Lagrangian particles that undergo cloud microphysics while interacting with the surrounding air. LCMs have been shown to overcome many problems faced by existing Eulerian models, including numerical diffusion (Grabowski et al., 2019; Hoffmann, 2016). LCMs have recently been used to successfully investigate detailed microphysical processes such as aerosol-cloud interactions (Andrejczuk et al., 2010; Hoffmann et al., 2015) or precipitation processes (Arabas & Shima, 2013; Dziekan & Pawlowska, 2017; Hoffmann et al., 2017; Naumann & Seifert, 2016).

Recently, Noh et al. (2018) obtained information about *A* by analyzing a box collision model, which used the collision scheme in the LCM. In this case, autoconversion was calculated directly by capturing the moments of the conversions of individual Lagrangian droplets from cloud droplets to raindrops. An analysis of the box collision model results, in which a lognormal DSD was assumed, revealed the relation as

$$A = \alpha q_c^{7/3} N_c^{-1/3} H(R_c - R_{c0}) \qquad (2)$$

which agreed with the results of Tripoli and Cotton (1980). Contrary to Tripoli and Cotton (1980), however, α increases linearly with the dissipation rate ε and the standard deviation of the DSD σ. Accordingly, α was parameterized as

$$\alpha = a(\sigma - \sigma_0)(1 + b\varepsilon)H(\sigma - \sigma_0), \qquad (3)$$

with a = 1.0 cm^{-1} μm^{-1} s^{-1} and b = 8.8 × 10^{-3} cm^{-2} s^{3}, where σ_0 is the threshold value of σ. However, in this parameterization, σ and ε are regarded as independent of q_c and N_c.

In the present work, we investigate how the effects of DSD and turbulence on *A* appear in realistic field simulations of shallow cumulus clouds using the LCM, in which the parameters are correlated. We carry out an extensive analysis of the correlations between parameters (Sections 3.2, 3.3, and 3.5), and propose how the effects of DSD and turbulence can be parameterized based on it, which results in a new parameterization of *A* (Section 3.4). We also investigate how exponent values of q_c and N_c vary when *A* is parameterized only in terms of q_c and N_c, as is done in many existing parameterizations (Section 3.6). The new parameterization is compared with the LCM data (Section 4.1) and applied to a bulk cloud model (BCM) while clarifying the difference between the cloud droplet mixing processes of the LCM and BCM (Section 4.2). The roles of DSD and turbulence in the parameterization of *A* are investigated by comparing the results from *A* with and without these effects (Section 4.1 and 4.3).

2 Model and Simulation

2.1 Lagrangian cloud models (LCM)

The employed LCM is the same as that used in Hoffmann et al. (2017) and Noh et al. (2018). To handle an extremely large number of cloud droplets, the concept of a super-droplet, which represents a large number of real droplets with identical features, is introduced. Each super-droplet moves under the influence of the turbulent flow field and the gravitational force while experiencing condensational and collisional growth. The turbulent flow field is calculated by an LES model, Parallelized Large-Eddy Simulation Model (PALM; Maronga et al., 2015; Raasch & Schröter, 2001). The collision scheme follows the algorithm introduced by Shima et al. (2009), in which collision occurs stochastically with the probability proportional to the collection kernel. The collision scheme is known to reproduce the realistic evolution of a cloud droplet spectrum (Unterstrasser et al., 2017). The collection kernel includes the effect of TICE (Ayala et al., 2008; Wang & Grabowski, 2009). One can refer to Hoffmann et al. (2017) and Noh et al. (2018) for a detailed explanation of the utilized LCM.

2.2 Bulk cloud model (BCM)

A new parameterization of *A* is applied to a BCM. The BCM employs the two-moment scheme of Morrison et al. (2005), the extension of Seifert and Beheng (2001, 2006), which predicts q_c, q_r, N_c, and N_r based on the assumption that the DSD follows a gamma distribution. Here, q_r and N_r are the mixing ratio and number concentration of raindrops, respectively. However, our parameterizations of the activation and condensational growth processes are different from those of Seifert and Beheng (2006). The number of activated aerosols is calculated by following the parameterization developed by Khvorostyanov and Curry (2006) for the prediction of N_c, and the increase in N_c is calculated by the difference between the predicted and existing N_c values at each time step. Condensational growth is parameterized by following Khairoutdinov and Kogan (2000). The BCM is already included in the PALM code, so the LCM and the BCM share the same dynamical core of LES, which enables direct comparisons among the effects of different cloud microphysical processes of LCM and BCM.

2.3 Simulation

We simulated shallow cumulus cloud fields based on the Barbados Oceanographic and Meteorological Experiment (BOMEX; Holland & Rassmusson, 1973). The initial profiles followed the LES intercomparison study (Siebesma et al., 2003) (Figure 1). To obtain information about autoconversion under various conditions, a large number of simulations were carried out with different initial cloud droplet concentrations and surface heat and moisture fluxes. Four different initial droplet number concentrations, N_0 = 60, 80, 100, and 120 cm^{-3}, were simulated, and these concentrations are referred to as N60, N80, N100, and N120, respectively. In addition to simulations with the original surface heat and moisture fluxes used for the BOMEX simulation ($\overline{w\theta}_0 = 8 \times 10^{-3}$ K m s^{-1} and $\overline{wq}_0 = 5.2 \times 10^{-5}$ m s^{-1}, respectively) (Siebesma et al., 2003), additional simulations with surface heat and moisture fluxes enhanced by 1.5 times were also carried out ($\overline{w\theta}_0 = 12 \times 10^{-3}$ K m s^{-1}, and $\overline{wq}_0 = 7.8 \times 10^{-5}$ m s^{-1}).

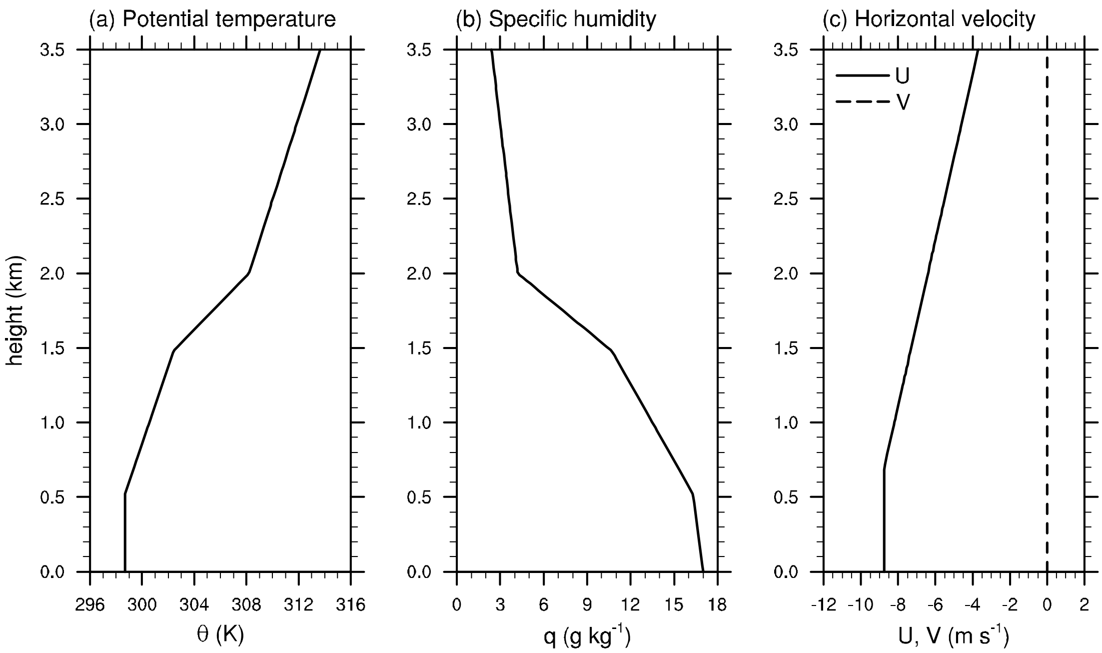

Figure 1 Initial environmental profiles for the BOMEX simulation.

In most simulations, the activation process, whose main contribution is to determine N_c, was bypassed to facilitate a large number of simulations while focusing on the collision process. The radii of all super-droplets were initially given by r = 0.01 μm, and the droplets were not allowed to evaporate and become any smaller. A time step of Δt = 0.2 s was used. Two simulations including the activation process with different aerosol concentrations (N_a = 120, 200 cm^{-3}) were also carried out to examine its possible effect and to conduct a comparison with the bulk model results. In this case, the initial distribution of aerosols followed the setting of Hoffmann et al. (2015), which was based on Derksen et al. (2009), and condensational growth included the contributions from curvature and solute effects with a much smaller time step.

The model grid spacing was set to 20 m in each direction, with a total of 120 × 120 × 144 grid points (2.4 km × 2.4 km × 2.88 km), to perform a large number of simulations of the computationally demanding LCM. We performed simulations with a larger domain size (4.8 km × 4.8 km × 2.88 km) and smaller grid size (10 m) for the N60 case to examine the model sensitivity (Appendix). This shows that the vertical profiles of variables and the general correlation patterns between parameters remained valid.

Integration was carried out for 6 hours, and the data obtained over the last 3 hours were used for analysis. Initially, 100 super-droplets were assigned to a grid, as this value is known to be sufficient for properly representing collisional growth (Arabas & Shima, 2013; Riechelmann et al., 2012; Unterstrasser et al., 2017).

2.4 Autoconversion calculation

We detected collision events between super-droplets at every time step. Every collision event was assigned to the autoconversion, accretion, or self-collection category, depending on the radii of the involved super-droplets before and after the collision (e.g., Noh et al., 2018). Only autoconversion was considered in the present work. The probability that autoconversion occurred at a single grid during one-time step (Δt = 0.2 s) was very small (10^{-5} – 5×10^{-4}).

The mass increases in raindrops from every collision event in a grid were added to calculate the average value of *A* under a given condition during the last 3 hours for all simulations (8 without activation and 2 with activation). The total number of grid data was approximately 2 million. For the calculation of $A(q_c, N_c, \sigma_c, \varepsilon)$, from the total grid data obtained over the last 3 hours, we collected grid data in which the parameters q_c, N_c, σ_c, and ε belonged to the same interval and regrouped them into a set $\{q_c, N_c, \sigma_c, \varepsilon\}$. Here, the standard deviation of the DSD of cloud droplets σ_c was used instead of that of the total droplets σ because the DSD does not follow an ideal distribution and raindrops do not affect autoconversion. $A(q_c, N_c, \sigma_c, \varepsilon)$ was then calculated by the average value of *A* over the grid data belonging to a given group $\{q_c, N_c, \sigma_c, \varepsilon\}$. The numbers of intervals for q_c, N_c, σ_c, and ε for a group $\{q_c, N_c, \sigma_c, \varepsilon\}$ were 50, 50, 50, and 50, respectively.

Regarding the separation radius between a cloud droplet and a raindrop, r^* = 25 μm was used, as in Noh et al. (2018), but the case with r^* = 40 μm was also analyzed. In the present simulations, autoconversion tended to be very small at r^* = 40 μm when N_0 was large.

3 Analysis of the LCM Results and a New parameterization

3.1 Evolution of clouds

Figure 2 shows the evolutions of the vertical profiles of horizontally averaged *A*, q_c, N_c / N_0, ε, σ_c, and R_c at N60, helping us to understand how various parameters contribute to autoconversion and how they are related to each other. Here, *A* and q_c are calculated by horizontal averaging as in previous results (e.g., Wyszogrodzki et al., 2013), but σ_c, ε, N_c / N_0, and R_c are averaged only within clouds with q_c > 10^{-5} kg kg^{-1}, as they are more relevant to autoconversion generation. ε is calculated directly from the LES (e.g., Riechelmann et al., 2012). Hereafter, all figures represent results obtained with the original surface heat and moisture fluxes unless otherwise specified. q_c appears at the cloud base and increases in magnitude while moving upward. Intermittently large values of *A*, q_c, and ε appear near the cloud top (e.g., *t* = 3, 4, 5.2 hours), which suggests that raindrops are formed at the top of a strong thermal with undiluted or slightly diluted cores (Khain et al. 2013).

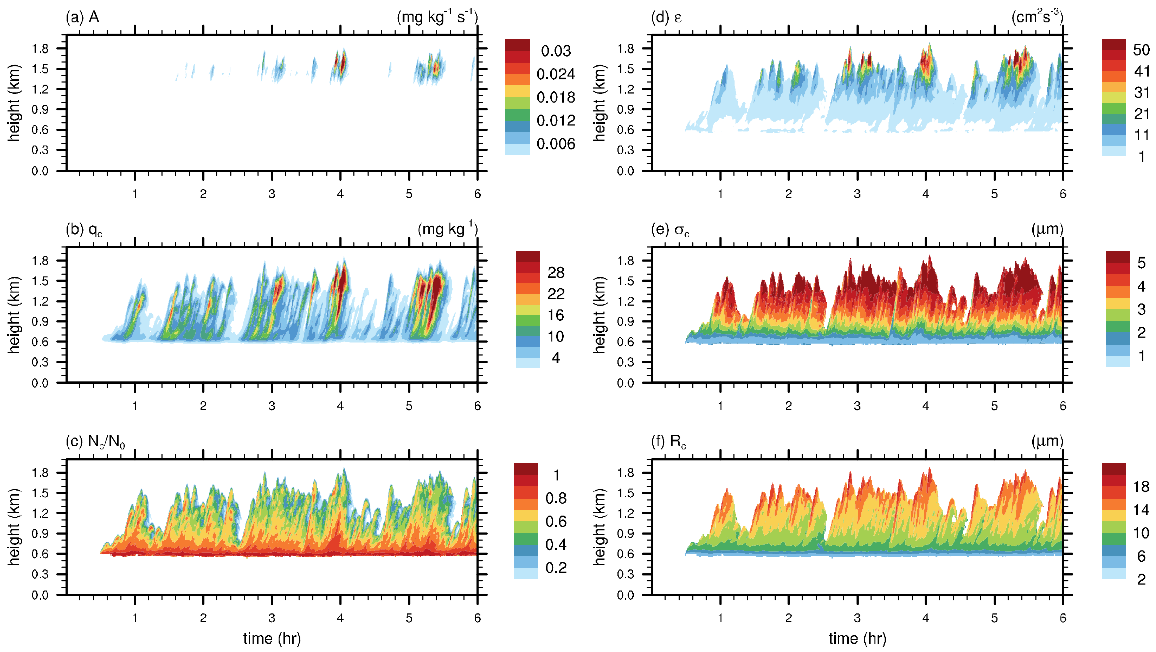

Figure 2 Time series of the horizontally averaged variables at N60: (a) *A*, (b) q_c, (c) N_c / N_0, (d) ε, (e) σ_c, (f) R_c (Here N_c / N_0, ε, σ_c, and R_c are averaged only within clouds.)

Figure 3 shows the horizontal mean vertical profiles of the corresponding parameters (A, q_c, N_c / N_0, ε, σ_c, and R_c), averaged over the last 3 hours of each simulation with different values of N_0. The profiles agree with previously obtained simulation results in general (Siebesma et al., 2003; Wyszogrodzki et al., 2013). All σ_c, R_c and ε increase with the height z within clouds, and ε becomes very large near the cloud top, as expected from Figure 2.

The stronger condensational growth at smaller N_0 values causes larger σ_c and R_c (Chandrakar et al., 2016; Grabowski & Wang, 2013). It is also found that the small increase in σ_c and R_c increases A greatly. On the other hand, q_c, ε and N_c / N_0 are less sensitive to N_0, as they are mainly controlled by cloud dynamics such as entrainment, mixing, and convection. Profiles of the cloud fraction, which will be shown in Figure 13, is also insensitive to N_0 either. The increases in q_c, ε, σ_c, and R_c with z and the decreases in σ_c, R_c, and A with N_0 suggest the presence of correlations between these parameters.

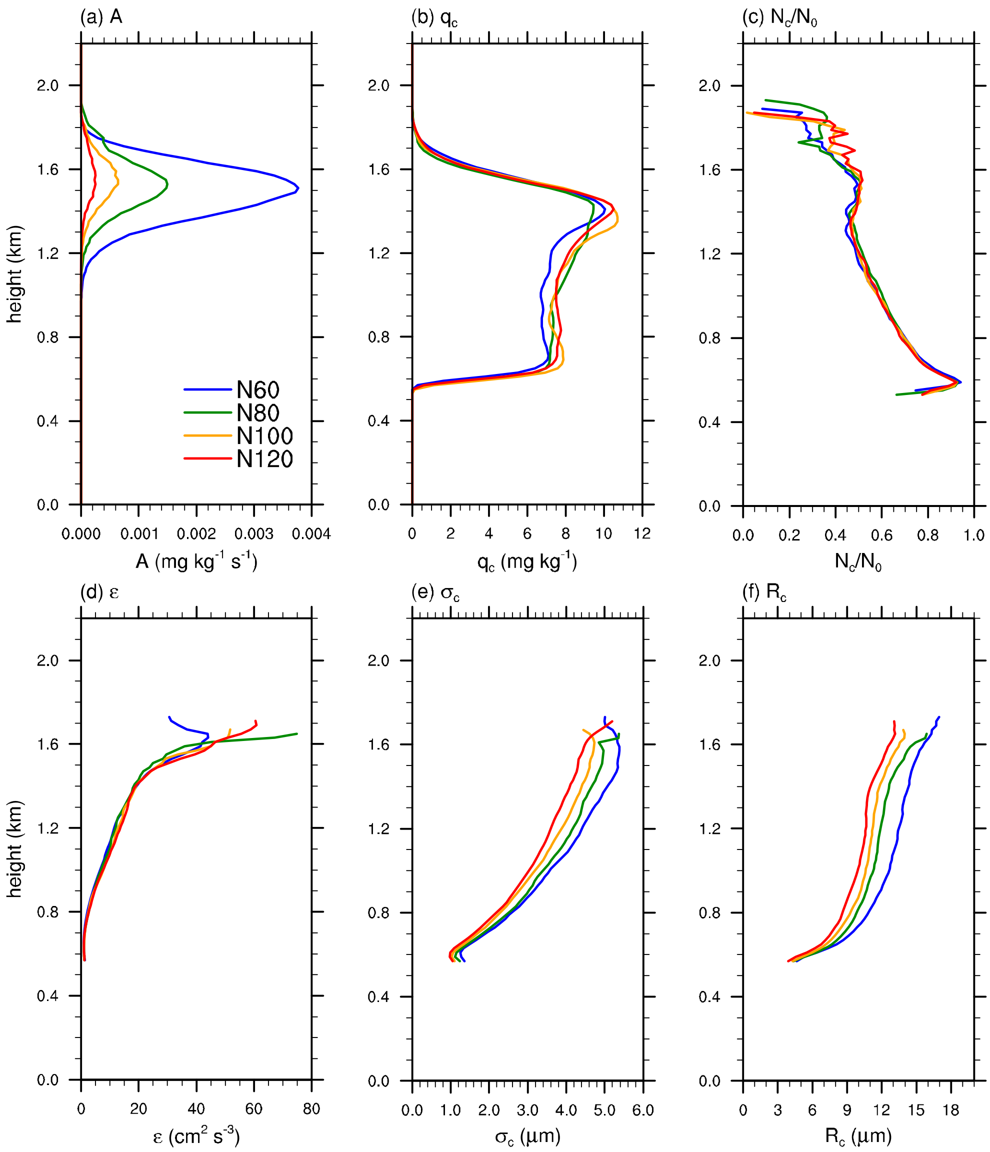

Figure 3 Vertical profiles of the horizontal mean variables averaged over the last 3 hours of simulations (blue: N60, green: N80, orange: N100, red: N120): (a) A, (b) q_c, (c) N_c / N_0, (d) ε, (e) σ_c, (f) R_c (Here N_c / N_0, ε, σ_c, and R_c are averaged only within clouds.)

3.2 Relation between σ_c and R_c

It is well known that the width of DSD tends to increase with the mean size of cloud droplets (Chandrakar et al., 2016; Cooper, 1989; Lasher-Trapp et al., 2005; Martin et al., 1994; Politovich, 1993; Shaw, 2003). Figures 2 and 3 also show that R_c and σ_c both increase with height. The broadening of the DSD may be caused by the different condensational growth histories of various droplets in the turbulent environment of a cloud affected by entrainment (Cooper, 1989; Lasher-Trapp et al., 2005; Luo et al., 2020; Shaw, 2003) or by the presence of collisional growth (Lu & Seinfeld, 2006).

Figure 4 shows the variations in the average standard deviations of the DSD for a given volume mean radius both for whole droplets (R_v, σ) and for cloud droplets smaller than r^* = 25 μm (R_c, σ_c). When R_v is small (R_v < 12 μm), σ increases linearly with R_v, while σ / R_v ($\simeq$ 0.3) is insensitive to N_0 (Figure 4a). Here, $\sigma / R_v \simeq 0.3$ is consistent with the values obtained from observation data (0.25 - 0.45), although the integral radius is used instead of R_v in those cases (Martin et al., 1994; Pawlowska et al., 2006; Politovich, 1993; Zhao et al., 2006). However, σ starts to grow more slowly with R_v at larger values of R_v (R_v > 12 μm), and ultimately, σ decreases with R_v. In this case, when N_0 is larger, the decrease in σ / R_v starts earlier, and σ becomes smaller.

The decrease in σ / R_v with N_0 is consistent with the findings of many previous reports (Chandrakar et al., 2016; Lu & Seinfeld, 2006; Martins & Silva Dias, 2009; Miles et al., 2000). The mass density distribution of droplets shows that the enhanced broadening of the DSD at lower N_0 is mainly attributed to the presence of stronger collisional growth (Figure 5), which is induced by stronger condensational growth.

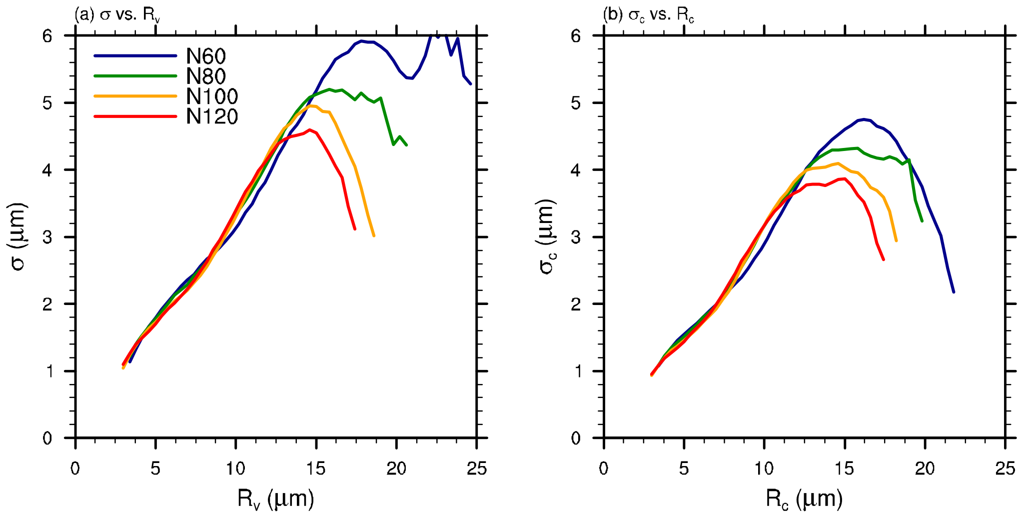

Figure 4 Variations in the mean standard deviation of the DSD with the volume mean radius (blue: N60, green: N80, orange: N100, and red: N120): (a) σ with R_v (whole droplets), (b) σ_c with R_c (only cloud droplets)

The decrease of σ with R_v at a large R_v value is related to the fact that droplets in the cloud core that are unaffected by entrainment tend to have larger R_v values but smaller σ values, while droplets near the cloud edge that are affected by entrainment tend to have smaller R_v values but larger σ values (Burnet & Brenguier, 2007; Hoffmann et al., 2017; Lasher-Trapp et al., 2005; Lu et al., 2013; Pardo et al., 2020; Tölle & Krueger, 2014).

When only cloud droplets are considered (Figure 4b), the variation pattern of σ_c with R_c is similar, but the decrease in σ_c with R_c starts earlier, thus decreasing the maximum σ_c. This phenomenon is due to the limiting effect induced by the threshold radius. That is, σ_c must approach zero as R_c approaches r^* because only droplets smaller than r^* are considered for the calculation of σ_c.

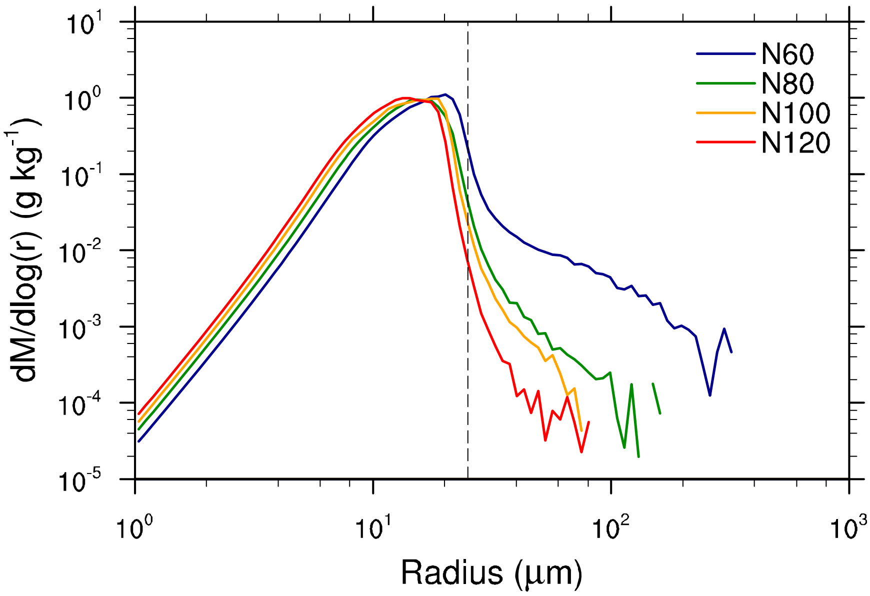

Figure 5 Mass density distributions of droplets (blue: N60, green: N80, orange: N100, and red: N120). A dashed vertical line represents $r^* = 25$ μm. The distributions are obtained from the data within clouds during the last 3 hours of simulations.

3.3 Variations in α with σ_c, R_c, ε, and N_c

Noh et al. (2018) showed that the relation $A \propto q_c^{7/3} N_c^{-1/3}$ is observed for given DSD and turbulence from an analysis of the box collision model results, as given by (2) (Figure 7 in Noh et al. (2018)). This relation implies the collisional growth of larger cloud droplets with R_c colliding gravitationally with smaller cloud droplets with no terminal velocity ($V_T \simeq 0$ m s^{-1}). The relation $A \propto q_c^{7/3} N_c^{-1/3}$ is obtained from $A \sim K N_c q_c$, $K \sim E R_c^2 V_T(R_c)$, and $V_T(R_c) \propto R_c^2$ following Stokes' law, if the collection efficiency E can be represented by the mean value (e.g., Liu & Daum, 2004; Tripoli & Cotton, 1980). Accordingly, we assume that the relation (2) remains valid for given DSD and turbulence, while α varies with DSD and turbulence, as in Noh et al. (2018). However, the correlations of DSD and turbulence with cloud parameters q_c and N_c can modify (3). Figure 5 also shows that the general pattern of the mass density distribution, which can be idealized by the lognormal or gamma distribution, is maintained regardless of the value of N_0 for cloud droplets.

Figure 6 shows the variations of α in (2) with σ_c and ε at different values of N_0 (= 60, 100 cm^{-3}), which is calculated by $A/(q_c^{7/3}N_c^{-1/3})$. The results show that α increases with σ_c and ε, as expected from (3). However, α is much larger at smaller N_0 values, as expected from Figure 3. The dependence on N_0 also represents the dependence on N_c since N_c/N_0 is almost independent of N_0 (Figure 3e). Figure 4 shows that R_c is larger for a given σ_c at R_c > 12 μm when N_0 is smaller. Therefore, a larger α at a smaller N_0 may suggest that α becomes larger at larger R_c, even if σ_c is the same.

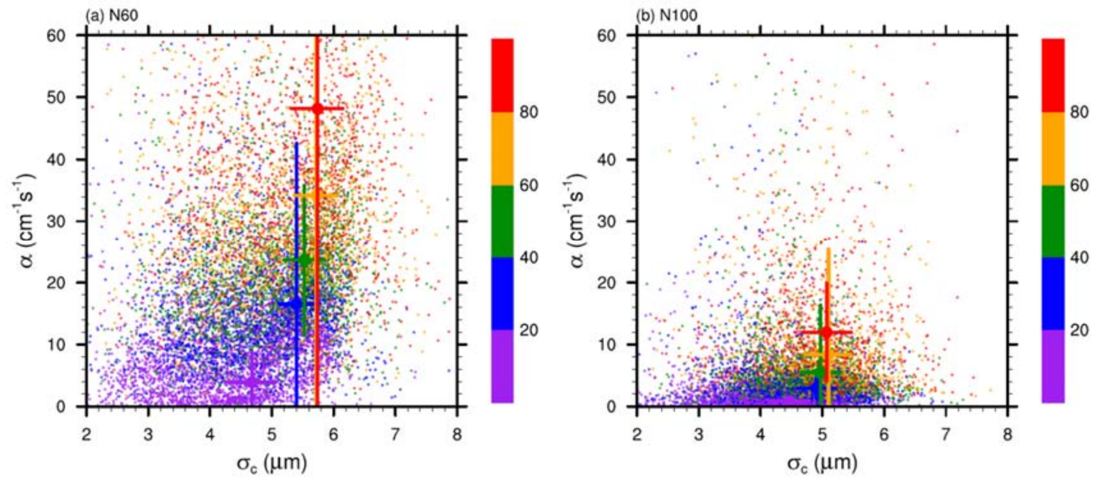

Figure 6 Scatter plots of α vs. σ_c (violet: 0 cm^2 s^{-3} ≤ ε < 20 cm^2 s^{-3}, blue: 20 cm^2 s^{-3} ≤ ε < 40 cm^2 s^{-3}, green: 40 cm^2 s^{-3} ≤ ε < 60 cm^2 s^{-3}, orange: 60 cm^2 s^{-3} ≤ ε < 80 cm^2 s^{-3}, red: 80 cm^2 s^{-3} ≤ ε < 100 cm^2 s^{-3}). The means (circles) and standard deviations (crosses) of α vs. σ_c are included: (a) N60, (b) N100.

The present result reveals that α depends on both R_c and σ_c, although the dependence on R_c was not considered in Noh et al. (2018). It implies that the variation of q_c and N_c with constant R_c gives $A \propto q_c^{7/3}N_c^{-1/3}$, but the tendency of increasing *E* with R_c (e.g., Long, 1974) can cause the increase of α with R_c. The effect of DSD thus means the effects of both R_c and σ_c hereafter in the present paper. In this case, the effect of DSD can also be represented in terms of R_c and N_c since σ_c/R_c varies with N_c (Figure 4). A parameterization in terms of σ_c appears somewhat unnatural, considering that two different groups of data with small and large values of R_c represent the same σ_c in Figure 4. More importantly, information about σ_c is not available from the atmospheric models. Therefore, it is more desirable to parameterize the effect of DSD in terms of R_c and N_c.

Figure 7 shows the variations in α with R_c and ε at different values of N_0 corresponding to Figure 6. α increases with R_c, starting at a certain value of R_c (= R_{c0}), and α is larger at smaller values of N_0, similar to Figure 6. This result also reflects the fact that σ_c is larger for the same R_c value (R_c > 12 μm) when N_0 is smaller (Figure 4). The values of R_{c0} are consistent with those used in Tripoli and Cotton (1980) (R_{c0} = 7 – 10 μm).

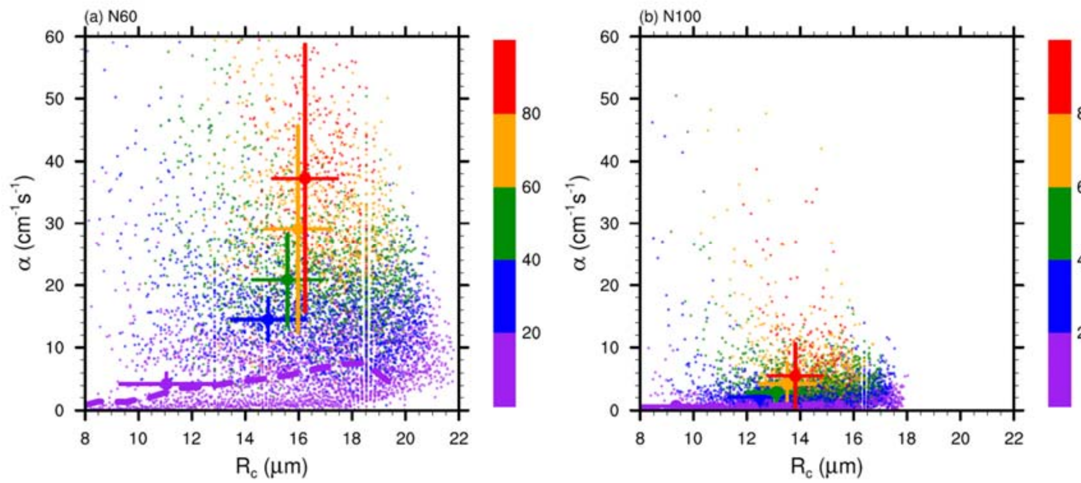

Figure 7 Scatter plots of α vs. R_c (violet: 0 cm^2 s^{-3} ≤ ε < 20 cm^2 s^{-3}, blue: 20 cm^2 s^{-3} ≤ ε < 40 cm^2 s^{-3}, green: 40 cm^2 s^{-3} ≤ ε < 60 cm^2 s^{-3}, orange: 60 cm^2 s^{-3} ≤ ε < 80 cm^2 s^{-3}, red: 80 cm^2 s^{-3} ≤ ε < 100 cm^2 s^{-3}). The means (circles) and standard deviations (crosses) of α vs. R_c are included. A dashed violet line represents the variation in the mean α with R_c for 0 cm^2 s^{-3} ≤ ε < 20 cm^2 s^{-3}: (a) N60, (b) N100.

It is important to mention that each data point in Figure 6 and 7 represents the average value of a set $\{q_c, N_c, \sigma_c, \varepsilon\}$, not the value at every grid, as explained in Section 2.4. On the other hand, the probability distribution functions of data show that the data with the radius near the mean value of R_c dominate for a given ε range (Figure 8). It means that most data are located within a range represented by the mean and standard deviation of R_c in Figure 7. Furthermore, large variations of α in Figure 6 and 7 reflect the fact that the characteristic of DSD is different depending on the location; that is, σ_c / R_c is large in the cloud core but small near the cloud edge affected by entrainment, as discussed in the previous section. For example, a small portion of data that shows large α at small R_c may represent the data from the cloud edge with large σ_c / R_c. However, Figure 8 shows that the contribution of scattered data away from the mean R_c to A is small. It should also be mentioned that α varies with ε significantly even within the same color range of ε in Figure 7.

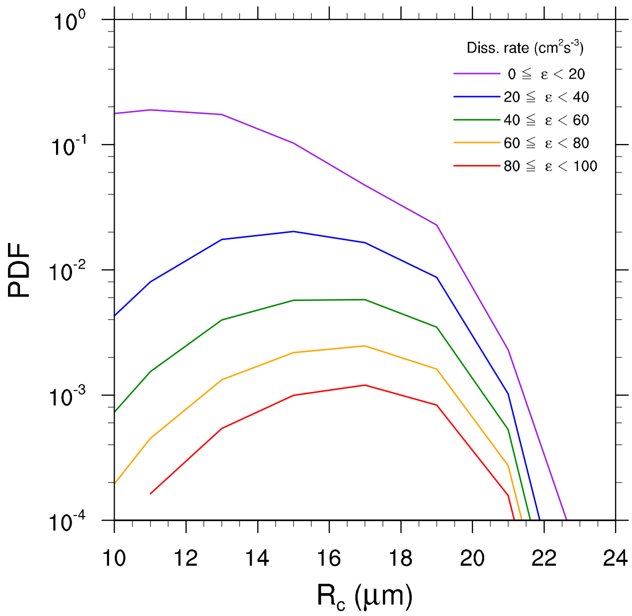

Figure 8 Probability distribution function of the data with R_c and ε at N60 (violet: 0 cm^2 s^{-3} ≤ ε < 20 cm^2 s^{-3}, blue: 20 cm^2 s^{-3} ≤ ε < 40 cm^2 s^{-3}, green: 40 cm^2 s^{-3} ≤ ε < 60 cm^2 s^{-3}, orange: 60 cm^2 s^{-3} ≤ ε < 80 cm^2 s^{-3}, red: 80 cm^2 s^{-3} ≤ ε < 100 cm^2 s^{-3}).

3.4 A new parameterization of *A*

Figure 7 shows the tendency of α to increase with R_c and ε but decrease with N_0. In particular, α increases linearly with $R_c - R_{c0}$ when the turbulence is weak (0 cm^2 s^{-3} ≤ ε < 20 cm^2 s^{-3}), while its slope decreases with N_0. Furthermore, Figure 4 suggests that σ_c / R_c becomes smaller at larger N_0 values in the range R_c > 12 μm, and this ratio dominates the contribution of the parameters to autoconversion. Based on these results, we can express the effect of DSD on α as $N_c^{-X}(R_c - R_{c0})$, instead of $(\sigma - \sigma_0)$ in (3), by using the proportionality of N_c to N_0 (Figure 3e).

The relation in (3) can then be rewritten as

$$\alpha = aN_c^{-X}(R_c - R_{c0})(1 + b\varepsilon)H(R_c - R_{c0}). \quad (5)$$

The best fit of the data, shown in Figure 7, provides X = 1.0, a = 8.0, b = 0.22 cm^{-2} s^3 and R_{c0} = 9 μm. Table 2 shows the optimal values of constants used in the parameterization (6) for both r^* = 25 and 40 μm. To obtain optimal coefficients, we first calculate $\alpha(q_c, N_c, \varepsilon)$ from the dataset $\{A, q_c, N_c, \varepsilon\}$ from all simulations, and regression analysis is carried out for $R_c - R_{c0}$ and $(R_c - R_{c0})\varepsilon$ with varying X and R_{c0}. The correlation of ε with q_c and N_c (or R_c), which will be discussed in the next section, is not parameterized here, because the information of ε can be obtained from the atmospheric models; especially, it can be obtained directly in LES (e.g., Heath et al., 2017; Huang et al., 2019).

Combining (5) with (2) results in the following:

$$A = aq_c^{7/3}N_c^{-(1/3+X)}(R_c - R_{c0})(1 + b\varepsilon)H(R_c - R_{c0}). \quad (6)$$

Noh et al. (2018) proposed the parameterization of the threshold radius R_{c0} in (2) as a function of σ based on the result of a box collision model. This parameterization cannot be applied anymore since σ_c and R_c are closely related, as shown in Figure 4. Instead, the threshold R_{c0} is included naturally in (6).

One important implication of the present result is that the dependence of the parameterization of A on q_c and N_c is generated via two different mechanisms. One derives from the collisional process based on gravitational collision for a given DSD, and the other is from the effects of DSD and turbulence and their correlations with q_c and N_c in real clouds. The box collision model results cannot provide information about the latter in general. Furthermore, one can also expect that exponential coefficients m and n in (1), as shown in Table 1, can differ depending on whether the effects of DSD and turbulence are considered explicitly or not.

r^* (μm)	X	a	b	R_{c0} (μm)
25	1.0	8.0	0.220	9
40	1.15	1.95	0.514	10

Table 2 Values of X, a, b and R_{c0} obtained via multiple regression analyses at r^* = 25 and 40 μm.

3.5 Relation between ε and σ_c

Another important feature in (5) is that b is substantially larger than previous estimations based on box collision model results (Franklin, 2008; Noh et al., 2018; Onishi et al., 2015; Seifert et al., 2010); for example, $b = 8.8 \times 10^{-3}$ cm^{-2} s^3 (Noh et al., 2018) or 1.5×10^{-3} cm^{-2} s^3 (Onishi et al., 2015).

Figure 9 shows that large values of ε are preferentially located in a region with larger σ_c and R_c values and in a region with larger σ_c values when R_c is held constant. This may reflect the fact that near the cloud top, where ε is larger, entrainment tends to increase σ_c. As a result, the effect of turbulence in (3) should be expressed as $(1+b_0\varepsilon)(1+b_1\varepsilon)$, where $1+b_0\varepsilon$ represents the effect of TICE and $1+b_1\varepsilon$ represents the effect of the preferential distribution of large ε values, i.e., σ_c tends to be larger at larger ε for a given R_c. As the simplest expression, $(1+b_0\varepsilon)(1+b_1\varepsilon)$ can be rewritten as $1+b\varepsilon$ with $b > b_0$. In the box collision model, in which there are no correlations between ε, σ_c, and R_c, the increase of A induced by ε represents only the effect of TICE.

The enhancement factor b_1 may vary with R_c, as suggested in Figure 9. Consequently, the relation between α and $R_c - R_{c0}$ is no longer linear at large values of ε, as suggested in Figure 7. Nonetheless, the variation of b with R_c is neglected for simplicity in the present parameterization because the data are concentrated in a narrow R_c range at large ε (Figure 8) and σ_c varies widely for a given R_c (Figure 9).

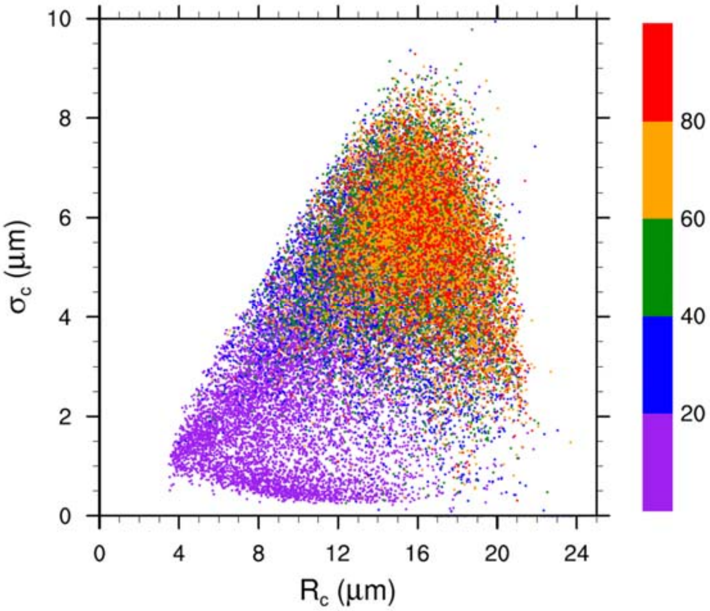

Figure 9 A scatter plot of σ_c vs. R_c at N60 (violet: 0 cm^2 s^{-3} $\leq \varepsilon <$ 20 cm^2 s^{-3}, blue: 20 cm^2 s^{-3} $\leq \varepsilon <$ 40 cm^2 s^{-3}, green: 40 cm^2 s^{-3} $\leq \varepsilon <$ 60 cm^2 s^{-3}, orange: 60 cm^2 s^{-3} $\leq \varepsilon <$ 80 cm^2 s^{-3}, red: 80 cm^2 s^{-3} $\leq \varepsilon <$ 100 cm^2 s^{-3}).

3.6 Effects of DSD and turbulence on the dependence of *A* on q_c and N_c

In many parameterizations, *A* is expressed only in terms of q_c and N_c (e.g., Beheng, 1994; Khairoutdinov & Kogan, 2000; Kogan, 2013; Liu & Daum, 2004; Tripoli & Cotton, 1980) (Table 1). The present result shows that *m* and *n* in (1) include the effects of DSD and turbulence, which, in turn, are affected by q_c and N_c. In particular, σ_c and R_c tend to decrease with N_c (Figure 4), and ε tends to increase with q_c (Figure 10). Consequently, *m* and *n* cannot be constant, but they should vary depending on the characteristics of the given cloud if *A* is expressed in terms of only q_c and N_c.

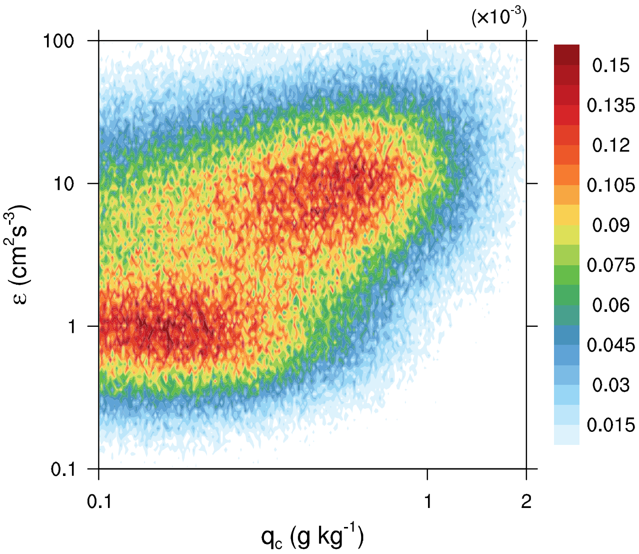

Figure 10 Probability distribution of the data in the $\varepsilon - q_c$ domain at N60 ($\Delta \log \varepsilon$ = 3.74 × 10^{-2} cm^2 s^{-3}, $\Delta \log q_c$ = 1.72 × 10^{-2} kg kg^{-1})

Figure 11 shows the variations in m and n in the ranges $3 < m < 4$ and $2 < n < 4$, respectively, when A is parameterized only in terms of q_c and N_c, i.e., $A \propto q_c^m N_c^{-n}$, using the least-squares method, as in Khairoutdinov and Kogan (2000). Here, we also include the results obtained regarding the surface heat and moisture fluxes enhanced by 1.5 times, in which the clouds develop to higher altitudes and result in larger ε, q_c, q_r, and R_c values. Figure 11 may explain the large variations in m and n (Table 1).

The parameterization given by (6) suggests that m and n in (1) should be larger than m = 7/3 and n = 1/3, respectively, when A is parameterized only in terms of q_c and N_c (e.g., Beheng (1994), Kogan (2013) in Table 1). The decrease in σ_c with increasing N_c (Figure 4) and the proportionality of N_c to N_0 (Figure 3e) make n larger than 1/3. The increase in ε with increasing q_c (Figure 10) makes m larger than 7/3. Figure 11 also suggests that n tends to be larger at higher aerosol concentrations and smaller surface fluxes because a smaller $R_c - R_{c0}$ in (6) is more sensitive to the variation in N_c.

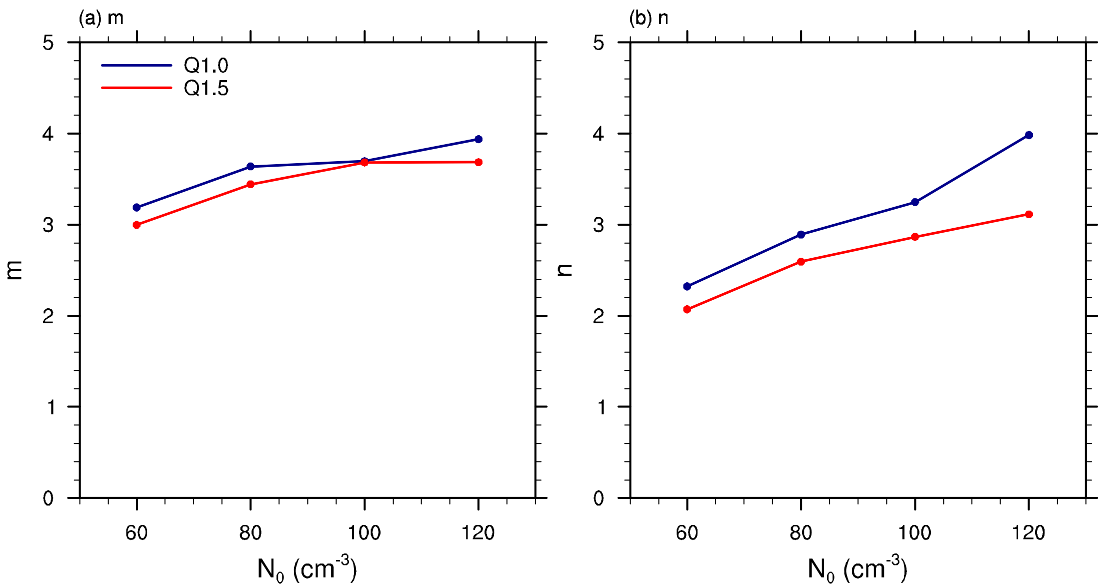

Figure 11 Variations in *m* and *n* with N_0 (blue: original surface heat and moisture fluxes; red: enhanced (1.5 times) surface heat and moisture fluxes).

4 Evaluation of the New Parameterization and the Effects of DSD and Turbulence

4.1 Comparison of the parameterizations of *A* with LCM data

Figure 12 compares the new parameterizations (NP) of *A* (6) with LCM data. To clarify the effects of DSD and turbulence on the parameterization of *A*, we also examine the cases in which their contributions are excluded in the parameterization; that is, constant values are used instead of $N_c^{-X}(R_c - R_{c0})$ and $(1+b\varepsilon)$ in (6), referred to as XDSD and XTURB, respectively. Here, the constant values are determined based on the averages of their corresponding in-cloud values. Furthermore, we include the parameterization obtained from the box collision model, in which there exist no correlations between the parameters ε, σ_c, and N_c (Noh et al., 2018), which is referred to as XCOR.

Since collisions occur stochastically with a probability that is proportional to the collection kernel in the LCM, only subgroups $\{q_c, N_c, \varepsilon\}$ with sufficiently large numbers of grid data have statistical significance. The criterion regarding the minimum number of grid data is set to 500 in

Figure 12 and Table 3. All data obtained from the simulations with and without the activation process are analyzed together since the difference is not significant compared to the differences among individual simulations. Note that the effect of the activation process is mainly limited to the determination of N_c.

NP shows a good correlation, which confirms that the formula and optimized constant values given by (6) indeed represent the LCM data properly. XDSD and XTURB result in more scattering and weaker correlation compared to NP (Table 3, Figure 12). In particular, they cannot produce large values of A (> 10^{-6} kg kg^{-1}s^{-1}), which represent intermittent bursts of raindrop formation near the cloud top under the influence of large R_c, σ_c, and ε (Figure 2). This illustrates the importance of the inclusion of the effects of DSD and turbulence on the parameterization of *A*. XCOR cannot reproduce large values of *A* either; this is partially attributed to the underestimation of *b*, which does not consider the correlation between turbulence and DSD.

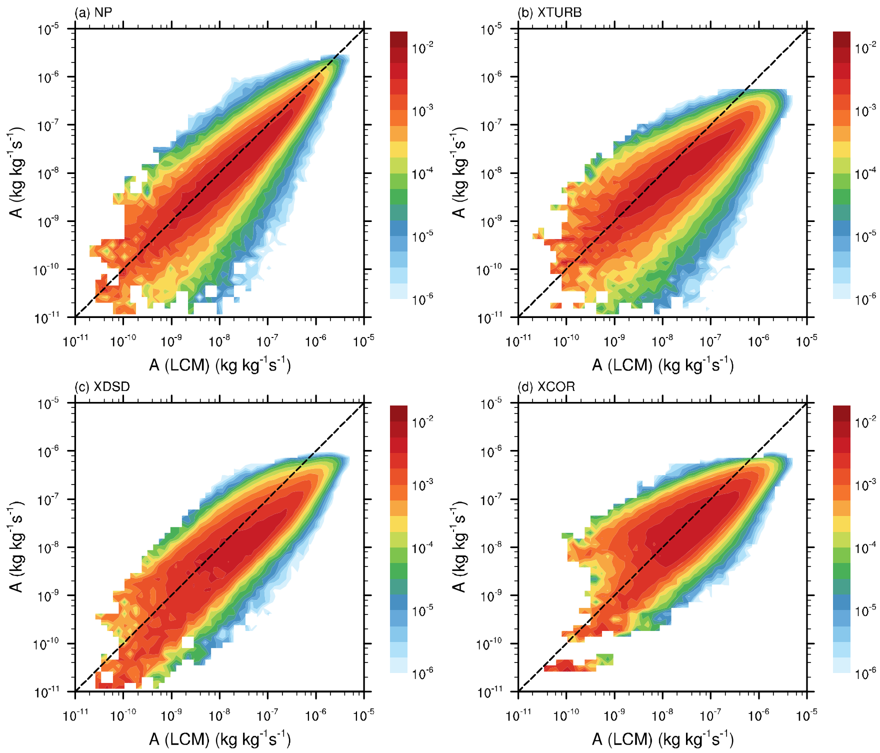

Figure 12 Probability distribution of A from the LCM data vs. bulk parameterizations (r^* = 25 μm): (a) NP, (b) XTURB, (c) XDSD, (d) XCOR.

	NP	XTURB	XDSD	XCOR
RMSE (10^{-8} kg kg^{-1} s^{-1})	4.52	7.88	7.28	6.90
correlation coefficient	0.77	0.59	0.58	0.53

Table 3 The root mean square errors (RMSEs) and correlation coefficients obtained from NP, XTURB, XDSD, and XCOR.

4.2 Application of the new parameterization to a BCM

It is important to understand how the parameterization of *A* affects the BCM results when it is applied to it. Figure 13 compares the profiles of various horizontal mean variables obtained from the LCM and the BCM with the new parameterization of *A*, similar to Figure 3. Additionally, the cases without the effects of DSD and turbulence (XDSD and XTURB, respectively) are included. Here, both the LCM and BCM simulations include the activation process that starts with an aerosol concentration N_a = 120 cm^{-3}.

Figure 13 shows that the differences between the LCM and BCM results appear not only in the profiles of *A* but also in various other profiles. Here, *A*, q_c, and cloud fraction are calculated by horizontal averaging, and σ_c, ε, N_c / N_0, and R_c are averaged only within clouds, similar to Figure 3. In the BCM, N_c does not decrease with *z*, and q_c does not increase near the cloud top; these findings are in contrast with the profiles obtained from the LCM. The contrast in the profiles of q_c and N_c agrees with the previous comparison of the LCM and BCM results conducted by Sato et al. (2018) for shallow cumulus cloud field simulations. This difference is attributed to the excessive turbulent diffusion of q_c and N_c across the cloud edge in the BCM, as suggested by Sato et al. (2018), causing a substantial loss of cloud droplets (or q_c and N_c) from the cloud in the BCM. This excessive loss of cloud droplets also eliminates the peak of q_c near the cloud top. However, the loss of N_c is immediately restored by the activation scheme in the BCM, in which the increase in N_c is calculated by the difference between the predicted and existing N_c values at every time step. This results in the overestimation of activation in the BCM, as pointed out by Hoffmann (2016). The LCM results show that the in-cloud activation is negligible in the present simulation (Hoffmann et al., 2015). Slawinska et al. (2012) also showed that in a BCM, N_c decreases as the height increases without activation above the cloud base, but it remains uniform with activation in shallow cumulus clouds.

As a result, the BCM makes N_c larger and q_c smaller as the height increases, and this leads to a slower increase in R_c with height than that provided by the LCM. The underestimation of q_c and R_c and the overestimation of N_c in the BCM cause the underestimation of *A*. Sato et al. (2018) showed that raindrops are formed from the LCM but not from the BCM. This suggests that the parameterization of the activation and condensation processes may require modification to match the LCM results, but this task is beyond the scope of the present paper. This fact also makes it difficult to evaluate the performance of the parameterizations of *A*. In this paper, we increase the proportional constant *a* in (6) by a factor of 2 as a way to cope with this difference, and the main focus is given to how the effects of DSD and turbulence in a parameterization affect the output result.

Figure 13 also shows that raindrop formation starts at heights that are too low in the BCM results. Too early onset of precipitation is also observed in the BCM compared to the SBM (Cotton & Anthes, 1989; Khain et al., 2015; Shipway & Hill, 2012; Straka & Rasmussen, 1997). This may also reflect the limitation of the BCM, in which *A* is calculated based on the mean values of parameters.

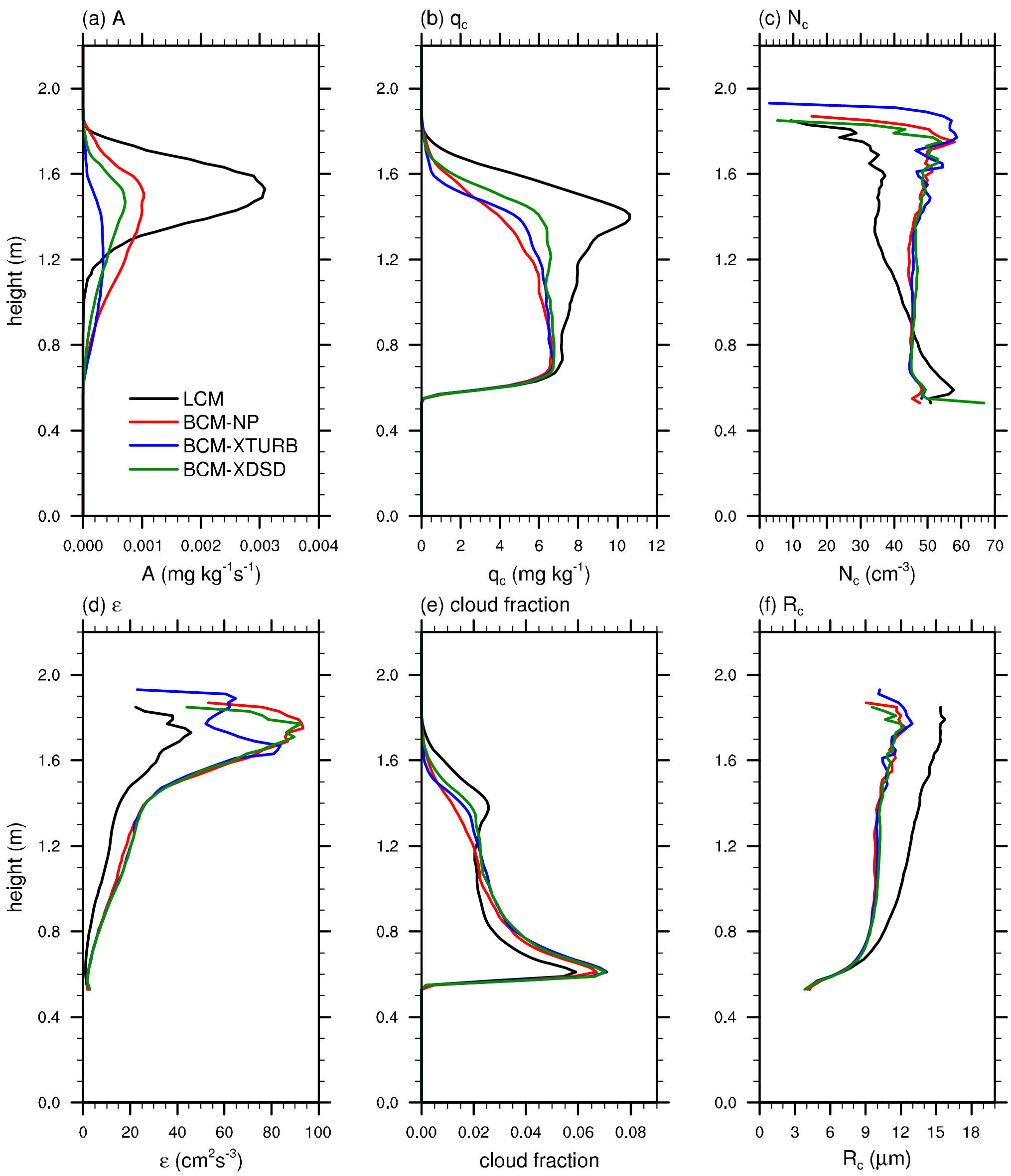

Figure 13 Vertical profiles of the horizontal mean variables averaged over the last 3 hours of simulations (black: LCM, red: BCM-NP, blue: BCM-XTURB, green: BCM-XDSD): (a) A, (b) q_c, (c) N_c, (d) ε, (e) cloud fraction, (f) R_c (Here N_c, ε, and R_c are averaged only within clouds.)

4.3 Effects of DSD and turbulence in a BCM

Figure 13 shows that *A* becomes much weaker when the effects of DSD and turbulence (XDSD and XTURB, respectively) are not included in the parameterization of *A*, although q_c and R_c are almost the same (or even slightly larger in the case of q_c). The effects of DSD and turbulence can be more clearly identified in the time series of q_c and *A* (Figure 14). It is difficult to reproduce intermittent bursts of raindrop formation with large values of *A*, as shown in Figure 2, without the effects of DSD or turbulence in the parameterization of *A* (XDSD, XTURB) (Table 4). This result is consistent with that shown in Figure 12, in which large values of *A* (> 10^{-6} kg kg^{-1}s^{-1}) cannot be reproduced in XDSD and XTURB. Figure 14 illustrates an important role of DSD and turbulence in the raindrop formation in shallow cumulus clouds, as shown by Hoffmann et al. (2017).

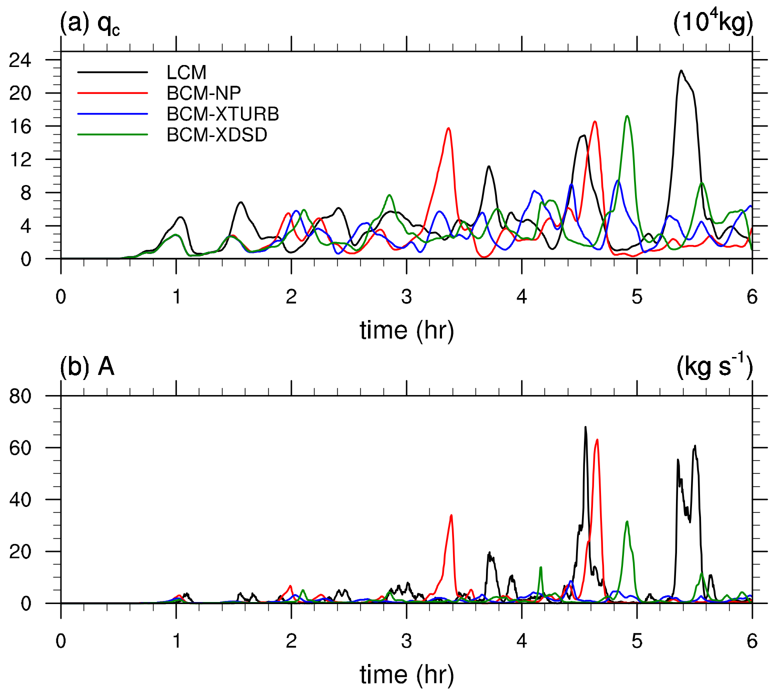

Figure 14 Time series of the vertically integrated (a) q_c, (b) *A* (black: LCM, red: BCM-NP, blue: BCM-XTURB, green: BCM-XDSD).

	q_c (10^8 kg)	A (10^4 kg)	A (> 20 kg s^{-1}) (10^4 kg)
LCM	1.49	2.16	1.82
NP	1.29	1.57	1.14
XTURB	1.15	0.56	0.01
XDSD	1.22	0.77	0.34

Table 4 Accumulated values of q_c, A, and A(> 20 kg s^{-1}).

5 Conclusions

In the present work, we investigated the roles of DSD and turbulence in A by analyzing the LCM data of shallow cumulus clouds. This goal was accomplished through the following steps while producing many results that have important implications for cloud microphysics.

First, the correlations of DSD and turbulence with cloud parameters q_c and N_c (or R_c) are investigated, and the results are applied to parameterize their effects in A. The physical meaning of a new parameterization of A is discussed.

- A new parameterization of A is developed as $A = \alpha q_c^{7/3} N_c^{-1/3} H(R_c - R_{c0})$ with $\alpha = aN_c^{-X}(R_c - R_{c0})(1 + b\varepsilon)$, where $A \propto q_c^{7/3} N_c^{-1/3}$ represents the collisional process based on gravitational collision for a given DSD and turbulence, and α represents the effects of DSD and turbulence ($N_c^{-X}(R_c - R_{c0})$ and $(1 + b\varepsilon)$, respectively). It reveals that the dependence of A on q_c and N_c is generated via these two different mechanisms. Analysis of a box collision model may not include the latter mechanism in general. The correlation of ε with q_c and N_c (or R_c) is not parameterized here, because the information of ε can be obtained from the atmospheric models.
- Both R_c and σ_c are found to affect α. The effect of DSD can be represented in terms of R_c and N_c since σ_c / R_c varies with N_c. α increases linearly with $R_c - R_{c0}$ when turbulence is weak, while the slope decreases with N_0 because of smaller σ_c / R_c. Based on this, the amplification effect of DSD on A is parameterized as $N_c^{-X}(R_c - R_{c0})$ with X = 1.0 and R_{c0} = 9 µm.

- Large values of ε are preferentially located in a region affected by entrainment, in which σ_c tends to be large for a given R_c. This makes *b* in the amplification effect of turbulence on *A*, $(1+b\varepsilon)$, much larger than that estimated from TICE.
- The effects of DSD and turbulence and their correlations with q_c and N_c explain a wide range of exponent values of q_c and N_c in many existing parameterizations of *A*.

Second, the new parameterization is compared with the LCM data, and applied to a bulk cloud model (BDM) while clarifying the difference between the cloud droplet mixing processes of the LCM and BCM. The roles of DSD and turbulence in the parameterization of *A* are investigated by comparing the results from *A* with and without these effects.

- The new parameterization of *A* is shown to exhibit a good correlation with LCM data. The parameterizations without the effects of DSD and turbulence show a lower correlation, and cannot produce large values of *A*.
- It is found from the comparison of the LCM and BCM results that the overestimation of the turbulent diffusion of q_c and N_c across the cloud edge in the BCM causes the overestimation of N_c due to excessive activation and the underestimation of q_c and R_c. This makes autoconversion more difficult in the BCM than in the LCM.
- An intermittent burst of raindrop formation with a large value of *A* can be reproduced by the new parameterization of *A*, but it cannot be reproduced without the inclusion of the effects of DSD and turbulence. It illustrates an important role of DSD and turbulence in the raindrop formation in shallow cumulus clouds.

Finally, it should be mentioned that the present work is based on the LCM results of shallows cumulus clouds. The correlation between parameters may vary depending on the given cloud conditions, and therefore, constant values in the parameterization (*X*, *a*, *b*, and R_{c0}), which are obtained for shallow cumulus clouds in the present study, can be modified for other clouds such as stratocumulus clouds and deep convective clouds. The comparison between the LCM and BCM results suggests that the optimization of the parameterization of *A* must be carried out in combination with the optimizations of other parameterizations, such as activation and condensation, because of the fundamental differences between cloud droplet mixing processes.

It also suggests the necessity for further comparison and evaluation of cloud microphysics reproduced by the LCM and SBM.

Appendix

To examine the validity of the LCM data used in the present study, it is necessary to investigate the sensitivities of the domain size and grid resolution in the LCM simulations. Figure A1 compares the vertical profiles of variables from the LCM simulations, corresponding to Figure 3, with a double horizontal domain size (DDS) of 4.8 km × 4.8 km × 2.88 km and a double grid resolution (DGR) of 10 m for the case of N60. The figure shows that the vertical profiles are hardly modified at DDS, but raindrop formation increases slightly with DGR; this is mainly because larger ε values are associated with better resolved convective eddies (Sato et al., 2018). The temporal variation in profiles becomes weaker at DDS as the number of generated clouds increases (not shown), but DDS does not affect the mean vertical profiles. The scatter plots of α vs. R_c, corresponding to Figure 7, also do not show significant differences (Figure A2). This confirms that the correlations between the parameters used for the parameterization of A (6) remain valid. At DGR, a larger ε can produce a larger A from the same parameterization (6).

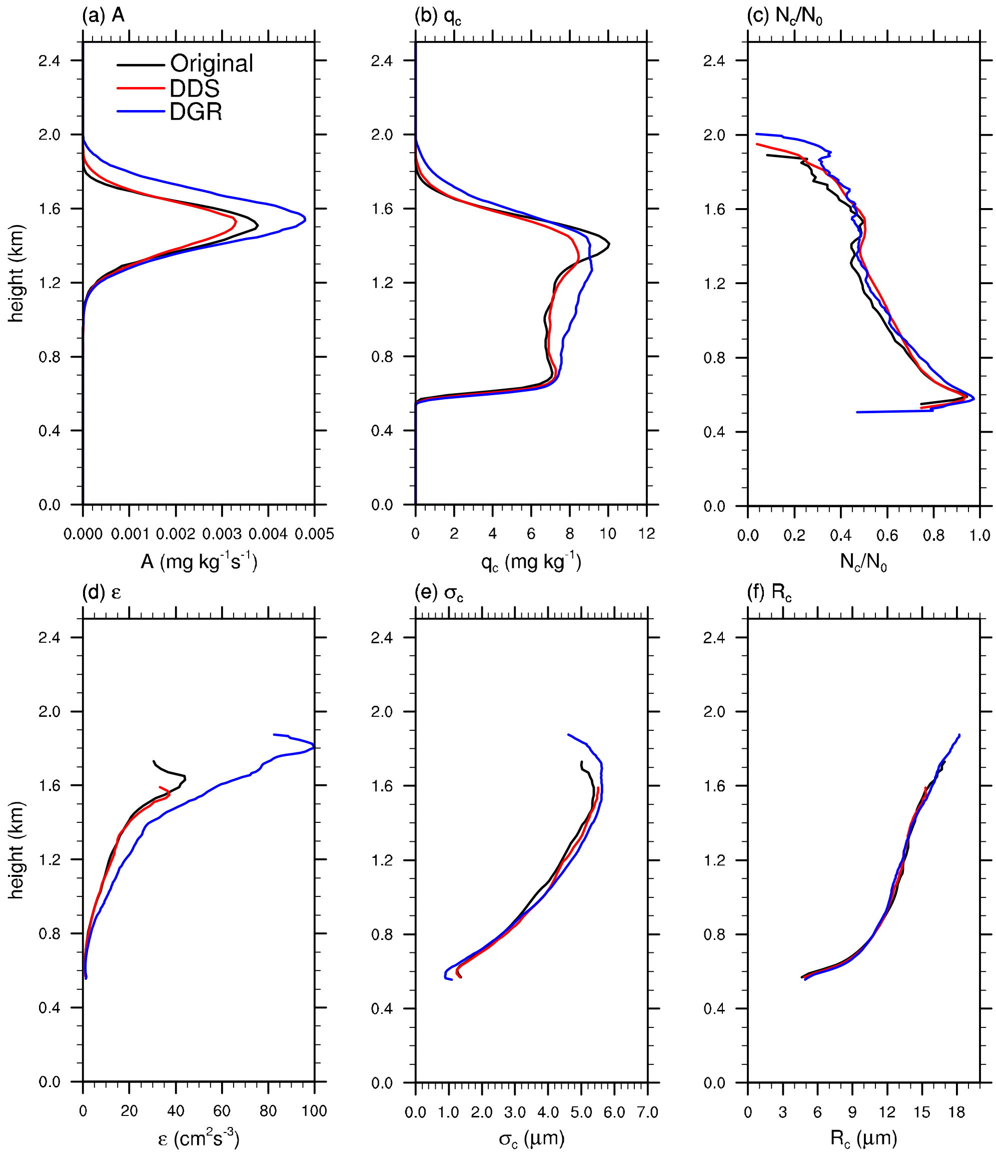

Figure A1 Vertical profiles of the variables averaged over the last 3 hours of simulations (black: original, red: DDS, blue: DGR): (a) A, (b) q_c, (c) N_c / N_0, (d) ε, (e) σ_c, (f) R_c (Here N_c / N_0, ε, σ_c, and R_c are averaged only within clouds.)

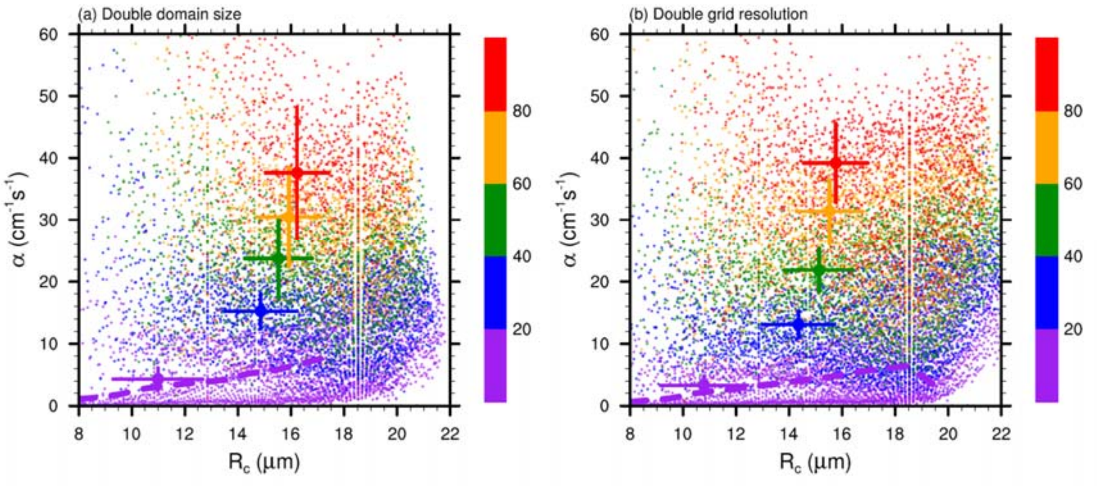

Figure A2 Scatter plots of α vs. R_c (violet: 0 cm^2 s^{-3} $\leq \varepsilon <$ 20 cm^2 s^{-3}, blue: 20 cm^2 s^{-3} $\leq \varepsilon <$ 40 cm^2 s^{-3}, green: 40 cm^2 s^{-3} $\leq \varepsilon <$ 60 cm^2 s^{-3}, orange: 60 cm^2 s^{-3} $\leq \varepsilon <$ 80 cm^2 s^{-3}, red: 80 cm^2 s^{-3} $\leq \varepsilon <$ 100 cm^2 s^{-3}). The means (circles) and standard deviations (crosses) of α vs. R_c are included. A dashed blue line represents the variation in the mean α with R_c for 0 cm^2 s^{-3} $\leq \varepsilon <$ 20 cm^2 s^{-3}: (a) DDS, (b) DGR.

Acknowledgments

This work was supported by the National Research Foundation of Korea (NRF) grant funded by the Korea government (MSIT) (No. 2021R1F1A1051121). This work was carried out by utilizing the supercomputer system at the National Center for Meteorological Supercomputer of Korea Meteorological Administration (KMA).

Data Availability Statement

This LES/LCM model used in this study is publicly available (https://palm.muk.uni-hannover.de/trac/browser?rev=4464). For analysis purposes, the model was extended, and additional analysis tools were developed. The code is available from the authors upon request. The data used for the figures in this paper are available at https://doi.org/10.6084/m9.figshare.14843004.v3

References

Andrejczuk, M., Grabowski, W., Reisner, J., & Gadian, A. (2010). Cloud-aerosol interactions for boundary layer stratocumulus in the Lagrangian Cloud Model. *Journal of Geophysical Research: Atmospheres*, 115, D22214. https://doi.org/10.1029/2010JD014248

Andrejczuk, M., Reisner, J., Henson, B., Dubey, M., & Jeffery, C. (2008). The potential impacts of pollution on a nondrizzling stratus deck: Does aerosol number matter more than type? *Journal of Geophysical Research: Atmospheres*, 113, D19204. https://doi.org/10.1029/2007JD009445

Arabas, S., Jaruga, A., Pawlowska, H., & Grabowski, W. W. (2015). libcloudph++ 1.0: a single-moment bulk, double-moment bulk, and particle-based warm-rain microphysics library in C++. *Geoscientific Model Development*, 8(6), 1677-1707. https://doi.org/10.5194/gmd-8-1677-2015

Arabas, S., & Shima, S.-i. (2013). Large-eddy simulations of trade wind cumuli using particle-based microphysics with Monte Carlo coalescence. *Journal of the Atmospheric Sciences*, 70(9), 2768-2777. https://doi.org/10.1175/JAS-D-12-0295.1

Ayala, O., Rosa, B., & Wang, L.-P. (2008). Effects of turbulence on the geometric collision rate of sedimenting droplets. Part 2. Theory and parameterization. *New Journal of Physics*, 10, 075016. https://doi.org/10.1088/1367-2630/10/7/075016

Baker, M., Corbin, R., & Latham, J. (1980). The influence of entrainment on the evolution of cloud droplet spectra: I. A model of inhomogeneous mixing. *Quarterly Journal of the Royal Meteorological Society*, 106(449), 581-598. https://doi.org/10.1002/qj.49710644914

Beheng, K. (1994). A parameterization of warm cloud microphysical conversion processes. *Atmospheric Research*, 33(1-4), 193-206. https://doi.org/10.1016/0169-8095(94)90020-5

Berry, E. X., & Reinhardt, R. L. (1974). An Analysis of Cloud Drop Growth by Collection Part II. Single Initial Distributions. *Journal of the Atmospheric Sciences*, 31(7), 1825-1831. https://doi.org/10.1175/1520-0469(1974)031<1825:AAOCDG>2.0.CO;2

Blyth, A. M. (1993). Entrainment in cumulus clouds. *Journal of Applied Meteorology and Climatology*, 32(4), 626-641. https://doi.org/10.1175/1520-0450(1993)032<0626:EICC>2.0.CO;2

Burnet, F., & Brenguier, J.-L. (2007). Observational study of the entrainment-mixing process in warm convective clouds. *Journal of the Atmospheric Sciences*, 64(6), 1995-2011.

https://doi.org/10.1175/JAS3928.1

Chandrakar, K. K., Cantrell, W., Chang, K., Ciochetto, D., Niedermeier, D., Ovchinnikov, M., et al. (2016). Aerosol indirect effect from turbulence-induced broadening of cloud-droplet size distributions. *Proceedings of the National Academy of Sciences*, 113(50), 14243-14248. https://doi.org/10.1073/pnas.1612686113

Cooper, W. A. (1989). Effects of variable droplet growth histories on droplet size distributions. Part I: Theory. *Journal of the Atmospheric Sciences*, 46(10), 1301-1311. https://doi.org/10.1175/1520-0469(1989)046<1301:EOVDGH>2.0.CO;2

Cotton, W.R. & Anthes, R.A. (1989). *Storms and Cloud Dynamics*, San Diego, CA: Academic Press.

Derksen, J., Roelofs, G.-J., & Röckmann, T. (2009). Influence of entrainment of CCN on microphysical properties of warm cumulus. *Atmospheric Chemistry and Physics*, 9(16), 6005-6015. https://doi.org/10.5194/acp-9-6005-2009

Dziekan, P., & Pawlowska, H. (2017). Stochastic coalescence in Lagrangian cloud microphysics. *Atmospheric Chemistry and Physics*, 17(22), 13509-13520. https://doi.org/10.5194/acp-17-13509-2017

Dziekan, P., Waruszewski, M., & Pawlowska, H. (2019). University of Warsaw Lagrangian Cloud Model (UWLCM) 1.0: a modern large-eddy simulation tool for warm cloud modeling with Lagrangian microphysics. *Geoscientific Model Development*, 12(6), 2587-2606. https://doi.org/10.5194/gmd-12-2587-2019

Franklin, C. N. (2008). A warm rain microphysics parameterization that includes the effect of turbulence. *Journal of the Atmospheric Sciences*, 65(6), 1795-1816. https://doi.org/10.1175/2007JAS2556.1

Grabowski, W. W., Morrison, H., Shima, S.-I., Abade, G. C., Dziekan, P., & Pawlowska, H. (2019). Modeling of cloud microphysics: Can we do better? *Bulletin of the American Meteorological Society*, 100(4), 655-672. https://doi.org/10.1175/BAMS-D-18-0005.1

Grabowski, W. W., & Wang, L.-P. (2013). Growth of cloud droplets in a turbulent environment. *Annual Review of Fluid Mechanics*, 45, 293-324. https://doi.org/10.1146/annurev-fluid-011212-140750

Heath, N. K., Fuelberg, H. E., Tanelli, S., Turk, F. J., Lawson, R. P., Woods, S., & Freeman, S. (2017). WRF nested large-eddy simulations of deep convection during SEAC4RS. *Journal* *of Geophysical Research: Atmospheres*, 122(7), 3953-3974. https://doi.org/10.1002/2016JD025465

Hoffmann, F. (2016). The effect of spurious cloud edge supersaturations in Lagrangian cloud models: An analytical and numerical study. *Monthly Weather Review*, 144(1), 107-118. https://doi.org/10.1175/MWR-D-15-0234.1

Hoffmann, F., Noh, Y., & Raasch, S. (2017). The route to raindrop formation in a shallow cumulus cloud simulated by a Lagrangian cloud model. *Journal of the Atmospheric Sciences*, 74(7), 2125-2142. https://doi.org/10.1175/JAS-D-16-0220.1

Hoffmann, F., Raasch, S., & Noh, Y. (2015). Entrainment of aerosols and their activation in a shallow cumulus cloud studied with a coupled LCM–LES approach. *Atmospheric Research*, 156, 43-57. https://doi.org/10.1016/j.atmosres.2014.12.008

Holland, J. Z., & Rasmusson, E. M. (1973). Measurements of the atmospheric mass, energy, and momentum budgets over a 500-kilometer square of tropical ocean. *Monthly Weather Review*, 101(1), 44-55. https://doi.org/10.1175/1520-0493(1973)101<0044:MOTAME>2.3.CO;2

Hsieh, W., Jonsson, H., Wang, L. P., Buzorius, G., Flagan, R., Seinfeld, J., & Nenes, A. (2009). On the representation of droplet coalescence and autoconversion: Evaluation using ambient cloud droplet size distributions. *Journal of Geophysical Research: Atmospheres*, 114, D07201. https://doi.org/10.1029/2008JD010502

Huang, Y., Liu, Y., Liu, Y., Li, H., & Knievel, J. C. (2019). Mechanisms for a record-breaking rainfall in the coastal metropolitan city of Guangzhou, China: Observation analysis and nested very large eddy simulation with the WRF model. *Journal of Geophysical Research: Atmospheres*, 124(3), 1370-1391. https://doi.org/10.1029/2018JD029668

Kessler, E. (1969). *On the distribution and continuity of water substance in atmospheric circulations*, Boston, MA: American Meteorological Society. https://doi.org/10.1007/978-1-935704-36-2_1

Khain, A., Beheng, K., Heymsfield, A., Korolev, A., Krichak, S., Levin, Z., et al. (2015). Representation of microphysical processes in cloud-resolving models: Spectral (bin) microphysics versus bulk parameterization. *Reviews of Geophysics*, 53(2), 247-322. https://doi.org/10.1002/2014RG000468

Khain, A., Prabha, T. V., Benmoshe, N., Pandithurai, G., & Ovchinnikov, M. (2013). The mechanism of first raindrops formation in deep convective clouds. *Journal of Geophysical*

Research: Atmospheres, 118(16), 9123-9140. https://doi.org/10.1002/jgrd.50641

Khairoutdinov, M., & Kogan, Y. (2000). A new cloud physics parameterization in a large-eddy simulation model of marine stratocumulus. *Monthly Weather Review*, 128(1), 229-243. https://doi.org/10.1175/1520-0493(2000)128<0229:ANCPPI>2.0.CO;2

Khvorostyanov, V. I., & Curry, J. A. (2006). Aerosol size spectra and CCN activity spectra: Reconciling the lognormal, algebraic, and power laws. *Journal of Geophysical Research: Atmospheres*, 111, D12202. https://doi.org/10.1029/2005JD006532

Kogan, Y. (2013). A cumulus cloud microphysics parameterization for cloud-resolving models. *Journal of the Atmospheric Sciences*, 70(5), 1423-1436. https://doi.org/10.1175/JAS-D-12-0183.1

Lasher-Trapp, S. G., Cooper, W. A., & Blyth, A. M. (2005). Broadening of droplet size distributions from entrainment and mixing in a cumulus cloud. *Quarterly Journal of the Royal Meteorological Society*, 131(605), 195-220. https://doi.org/10.1256/qj.03.199

Lee, H., & Baik, J.-J. (2017). A physically based autoconversion parameterization. *Journal of the Atmospheric Sciences*, 74(5), 1599-1616. https://doi.org/10.1175/JAS-D-16-0207.1

Liu, Y., & Daum, P. H. (2004). Parameterization of the autoconversion process. Part I: Analytical formulation of the Kessler-type parameterizations. *Journal of the Atmospheric Sciences*, 61(13), 1539-1548. https://doi.org/10.1175/1520-0469(2004)061<1539:POTAPI>2.0.CO;2

Liu, Y., Daum, P. H., McGraw, R. L., Miller, M. A., & Niu, S. (2007). Theoretical expression for the autoconversion rate of the cloud droplet number concentration. *Geophysical Research Letters*, 34, L16821. https://doi.org/10.1029/2007GL030389

Long, A. B. (1974), Solutions to droplet collection equation for polynomial kernels, J. Atmos. Sci., 31, 1040–1052. https://doi.org/10.1175/1520-0469(1974)031<1040:STTDCE>2.0.CO;2

Lu, C., Niu, S., Liu, Y., & Vogelmann, A. M. (2013). Empirical relationship between entrainment rate and microphysics in cumulus clouds. *Geophysical Research Letters*, 40(10), 2333-2338. https://doi.org/10.1002/grl.50445

Lu, M. L., & Seinfeld, J. H. (2006). Effect of aerosol number concentration on cloud droplet dispersion: A large-eddy simulation study and implications for aerosol indirect forcing. *Journal of Geophysical Research: Atmospheres*, 111, D02207. https://doi.org/10.1029/2005JD006419

Luo, S., Lu, C., Liu, Y., Bian, J., Gao, W., Li, J., et al. (2020). Parameterizations of entrainment-mixing mechanisms and their effects on cloud droplet spectral width based on numerical simulations. *Journal of Geophysical Research: Atmospheres*, 125, e2020JD032972. https://doi.org/10.1029/2020JD032972

Maronga, B., Gryschka, M., Heinze, R., Hoffmann, F., Kanani-Sühring, F., Keck, M., et al. (2015). The Parallelized Large-Eddy Simulation Model (PALM) version 4.0 for atmospheric and oceanic flows: model formulation, recent developments, and future perspectives. *Geoscientific Model Development*, 8(8), 2515-2551. https://doi.org/10.5194/gmd-8-2515-2015

Martin, G., Johnson, D., & Spice, A. (1994). The measurement and parameterization of effective radius of droplets in warm stratocumulus clouds. *Journal of the Atmospheric Sciences*, 51(13), 1823-1842. https://doi.org/10.1175/1520-0469(1994)051<1823:TMAPOE>2.0.CO;2

Martins, J., & Silva Dias, M. (2009). The impact of smoke from forest fires on the spectral dispersion of cloud droplet size distributions in the Amazonian region. *Environmental Research Letters*, 4(1), 015002. https://doi.org/10.1088/1748-9326/4/1/015002

Menon, S., Brenguier, J. L., Boucher, O., Davison, P., Del Genio, A. D., Feichter, J., et al. (2003). Evaluating aerosol/cloud/radiation process parameterizations with single-column models and Second Aerosol Characterization Experiment (ACE-2) cloudy column observations. *Journal of Geophysical Research: Atmospheres*, 108(D24), 4762. https://doi.org/10.1029/2003JD003902

Milbrandt, J., & Yau, M. (2005). A multimoment bulk microphysics parameterization. Part I: Analysis of the role of the spectral shape parameter. *Journal of the Atmospheric Sciences*, 62(9), 3051-3064. https://doi.org/10.1175/JAS3534.1

Milbrandt, J., & Yau, M. (2005). A multimoment bulk microphysics parameterization. Part II: A proposed three-moment closure and scheme description. *Journal of the Atmospheric Sciences*, 62(9), 3065-3081. https://doi.org/10.1175/JAS3535.1

Miles, N. L., Verlinde, J., & Clothiaux, E. E. (2000). Cloud droplet size distributions in low-level stratiform clouds. *Journal of the Atmospheric Sciences*, 57(2), 295-311. https://doi.org/10.1175/1520-0469(2000)057<0295:CDSDIL>2.0.CO;2

Morrison, H., Curry, J., & Khvorostyanov, V. (2005). A new double-moment microphysics parameterization for application in cloud and climate models. Part I: Description. *Journal of the Atmospheric Sciences*, 62(6), 1665-1677. https://doi.org/10.1175/JAS3446.1

Naumann, A. K., & Seifert, A. (2016). Evolution of the shape of the raindrop size distribution in simulated shallow cumulus. *Journal of the Atmospheric Sciences*, 73(6), 2279-2297. https://doi.org/10.1175/JAS-D-15-0263.1

Noh, Y., Oh, D., Hoffmann, F., & Raasch, S. (2018). A cloud microphysics parameterization for shallow cumulus clouds based on Lagrangian cloud model simulations. *Journal of the Atmospheric Sciences*, 75(11), 4031-4047. https://doi.org/10.1175/JAS-D-18-0080.1

Onishi, R., Matsuda, K., & Takahashi, K. (2015). Lagrangian tracking simulation of droplet growth in turbulence–turbulence enhancement of autoconversion rate. *Journal of the Atmospheric Sciences*, 72(7), 2591-2607. https://doi.org/10.1175/JAS-D-14-0292.1

Pardo, L. H., Morrison, H., Machado, L. A., Harrington, J. Y., & Lebo, Z. J. (2020). Drop size distribution broadening mechanisms in a bin microphysics Eulerian model. *Journal of the Atmospheric Sciences*, 77(9), 3249-3273. https://doi.org/10.1175/JAS-D-20-0099.1

Pawlowska, H., Grabowski, W. W., & Brenguier, J. L. (2006). Observations of the width of cloud droplet spectra in stratocumulus. *Geophysical Research Letters*, 33, L19810. https://doi.org/10.1029/2006GL026841

Pinsky, M., & Khain, A. (2002). Effects of in-cloud nucleation and turbulence on droplet spectrum formation in cumulus clouds. *Quarterly Journal of the Royal Meteorological Society*, 128(580), 501-533. https://doi.org/10.1256/003590002321042072

Politovich, M. K. (1993). A study of the broadening of droplet size distributions in cumuli. *Journal of the Atmospheric Sciences*, 50(14), 2230-2244. https://doi.org/10.1175/1520-0469(1993)050<2230:ASOTBO>2.0.CO;2

Raasch, S., & Schröter, M. (2001). PALM–A large-eddy simulation model performing on massively parallel computers. *Meteorologische Zeitschrift*, 10, 363-372. https://doi.org/10.1127/0941-2948/2001/0010-0363

Riechelmann, T., Noh, Y., & Raasch, S. (2012). A new method for large-eddy simulations of clouds with Lagrangian droplets including the effects of turbulent collision. *New Journal of Physics*, 14, 065008. https://doi.org/10.1088/1367-2630/14/6/065008

Sato, Y., Shima, S. i., & Tomita, H. (2018). Numerical convergence of shallow convection cloud field simulations: Comparison between double-moment Eulerian and particle-based Lagrangian microphysics coupled to the same dynamical core. *Journal of Advances in Modeling Earth Systems*, 10(7), 1495-1512. https://doi.org/10.1029/2018MS001285

Seifert, A., & Beheng, K. D. (2001). A double-moment parameterization for simulating autoconversion, accretion and selfcollection. *Atmospheric Research*, 59, 265-281. https://doi.org/10.1016/S0169-8095(01)00126-0

Seifert, A., & Beheng, K. D. (2006). A two-moment cloud microphysics parameterization for mixed-phase clouds. Part 1: Model description. *Meteorology and Atmospheric Physics*, 92(1), 45-66. https://doi.org/10.1007/s00703-005-0112-4

Seifert, A., Nuijens, L., & Stevens, B. (2010). Turbulence effects on warm-rain autoconversion in precipitating shallow convection. *Quarterly Journal of the Royal Meteorological Society*, 136(652), 1753-1762. https://doi.org/10.1002/qj.684

Seifert, A., & Onishi, R. (2016). Turbulence effects on warm-rain formation in precipitating shallow convection revisited. *Atmospheric Chemistry and Physics*, 16(18), 12127-12141. https://doi.org/10.5194/acp-16-12127-2016

Shaw, R. A. (2003). Particle-turbulence interactions in atmospheric clouds. *Annual Review of Fluid Mechanics*, 35(1), 183-227. https://doi.org/10.1146/annurev.fluid.35.101101.161125

Shima, S.-i., Kusano, K., Kawano, A., Sugiyama, T., & Kawahara, S. (2009). The super-droplet method for the numerical simulation of clouds and precipitation: A particle-based and probabilistic microphysics model coupled with a non-hydrostatic model. *Quarterly Journal of the Royal Meteorological Society*, 135(642), 1307-1320. https://doi.org/10.1002/qj.441

Shipway, B., & Hill, A. (2012). Diagnosis of systematic differences between multiple parametrizations of warm rain microphysics using a kinematic framework. *Quarterly Journal of the Royal Meteorological Society*, 138(669), 2196-2211. https://doi.org/10.1002/qj.1913

Siebesma, A. P., Bretherton, C. S., Brown, A., Chlond, A., Cuxart, J., Duynkerke, P. G., et al. (2003). A large eddy simulation intercomparison study of shallow cumulus convection. *Journal of the Atmospheric Sciences*, 60(10), 1201-1219. https://doi.org/10.1175/1520-0469(2003)60<1201:ALESIS>2.0.CO;2

Slawinska, J., Grabowski, W. W., Pawlowska, H., & Morrison, H. (2012). Droplet activation and mixing in large-eddy simulation of a shallow cumulus field. *Journal of the Atmospheric Sciences*, 69(2), 444-462. https://doi.org/10.1175/JAS-D-11-054.1

Sölch, I., & Kärcher, B. (2010). A large-eddy model for cirrus clouds with explicit aerosol and ice microphysics and Lagrangian ice particle tracking. *Quarterly Journal of the Royal Meteorological Society*, 136(653), 2074-2093. https://doi.org/10.1002/qj.689

Straka, J. M., & Rasmussen, E. N. (1997). Toward improving microphysical parameterizations of conversion processes. *Journal of Applied Meteorology*, 36(7), 896-902. https://doi.org/10.1175/1520-0450(1997)036<0896:TIMPOC>2.0.CO;2

Tölle, M. H., & Krueger, S. K. (2014). Effects of entrainment and mixing on droplet size distributions in warm cumulus clouds. *Journal of Advances in Modeling Earth Systems*, 6(2), 281-299. https://doi.org/10.1002/2012MS000209

Tripoli, G. J., & Cotton, W. R. (1980). A Numerical Investigation of Several Factors Contributing to the Observed Variable Intensity of Deep Convection over South Florida. *Journal of Applied Meteorology and Climatology*, 19(9), 1037-1063. 10.1175/1520-0450(1980)019<1037:Aniosf>2.0.Co;2

Unterstrasser, S., Hoffmann, F., & Lerch, M. (2017). Collection/aggregation algorithms in Lagrangian cloud microphysical models: Rigorous evaluation in box model simulations. *Geoscientific Model Development*, 10(4), 1521-1548. https://doi.org/10.5194/gmd-10-1521-2017

Wang, L. P., & Grabowski, W. W. (2009). The role of air turbulence in warm rain initiation. *Atmospheric Science Letters*, 10(1), 1-8. https://doi.org/10.1002/asl.210

Wood, R. (2005). Drizzle in stratiform boundary layer clouds. Part II: Microphysical aspects. *Journal of the Atmospheric Sciences*, 62(9), 3034-3050. https://doi.org/10.1175/JAS3530.1

Wyszogrodzki, A., Grabowski, W., Wang, L.-P., & Ayala, O. (2013). Turbulent collision-coalescence in maritime shallow convection. *Atmospheric Chemistry and Physics*, 13(16), 8471-8487. https://doi.org/10.5194/acp-13-8471-2013

Zhao, C., Tie, X., Brasseur, G., Noone, K. J., Nakajima, T., Zhang, Q., et al. (2006). Aircraft measurements of cloud droplet spectral dispersion and implications for indirect aerosol radiative forcing. *Geophysical Research Letters*, 33, L16809. https://doi.org/10.1029/2006GL026653